CRYSTAL GROWTH & DESIGN

pubs.acs.org/crystal

Article

Novel Purine Alkaloid Cocrystals with Trimesic and Hemimellitic Acids as Coformers: Synthetic Approach and Supramolecular Analysis

M. R. Gołdyn,* D. Larowska, and E. Bartoszak-Adamska

Cite This: *Cryst. Growth Des.* 2021, 21, 396−413

Read Online

ACCESS | Metrics & More | Article Recommendations | Supporting Information

ABSTRACT: In this work, benzene-1,3,5-tricarboxylic (trimesic acid, TMSA) and benzene-1,2,3-tricarboxylic acid (hemimellitic acid, HMLA) were used as coformers for cocrystal synthesis with chosen purine alkaloids. Theobromine (TBR) forms cocrystals TBR·TMSA and TBR·HMLA with these acids. Theophylline (TPH) forms cocrystals TPH·TMSA and TPH·HMLA, the cocrystal hydrate TPH·TMSA·2H_2O and the salt hydrate $(TPH)^+\cdot(HMLA)^-\cdot 2H_2O$. Caffeine (CAF) forms the cocrystal CAF·TMSA and the cocrystal hydrate CAF·HMLA·H_2O. The purine alkaloid derivatives were obtained by solution crystallization and by neat or liquid-assisted grinding. The powder X-ray diffraction method was used to confirm the synthesis of the novel substances. All of these solids were structurally characterized, and all synthons formed by purine alkaloids and carboxylic acids were recognized using a single-crystal X-ray diffraction method. The Cambridge Structural Database was used to determine the frequency of occurrence of analyzed supramolecular synthons, which is essential at the crystal structure design stage. Determining the influence of structural causes on the various synthon formations and molecular arrangements in the crystal lattice was possible using structurally similar purine alkaloids and two isomers of benzenetricarboxylic acid. Additionally, UV−vis measurements were made to determine the effect of cocrystallization on purine alkaloid solubility.

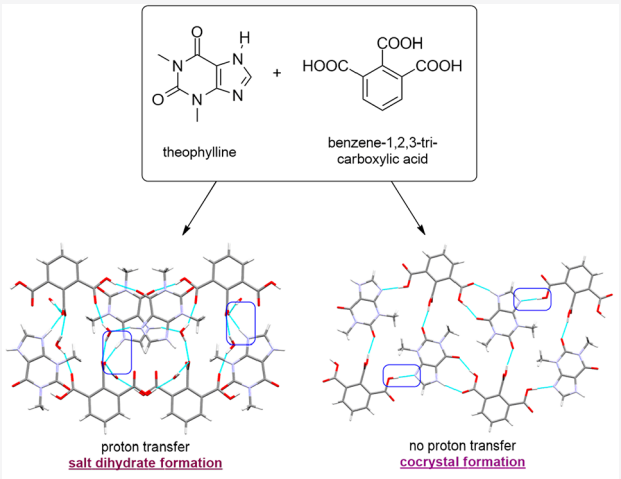

1. INTRODUCTION

Cocrystals, two- or multiple-component solids containing substances that are also solids under neutral conditions, are gaining increasing interest, especially in the pharmaceutical industry, where one of the components is the pharmaceutically active ingredient (API).[1−3] These complex systems arise spontaneously as a result of component interactions using noncovalent, intermolecular, reversible interactions, i.e., hydrogen bonds, $\pi\cdots\pi$, or van der Waals forces.[2,4,5] In this way there are modifications of the molecular arrangement in the crystal lattice. The aggregates formed usually have properties different from those of the substances that are part of the molecular complex.[6−10] From a pharmaceutical point of view, the water solubility and permeability are some of the most important properties of a given substance that determine its clinical effectiveness.[11−14] These two properties assign a drug to a specific group in the biopharmaceutical classification system (BCS), which in turn allows a choice of a suitable method to improve the properties of a given drug.[15−18] There are many physical (particle size reduction, mechanical micronization, solid dispersion, and nanoparticles) and chemical methods (formation of cocrystals, salts, and solvates and search for polymorphs) to modify the properties of the API.[11,19−22] Around 60−70% of the discovered drugs belong to the BCS classes II (low solubility and high permeability) and IV (low solubility and low permeability), which means that it is essential to search for appropriate methods of drug modification that will eliminate the difficulties associated with unfavorable drug properties: i.e., solubility, stability, or therapeutic effectiveness. One of the most effective ways to improve the physicochemical properties of a drug is pharmaceutical cocrystallization, which consists of introducing guest molecules (coformers) into the API's crystal lattice.[23,24] Among other important physicochemical properties, in addition to solubility, that can be improved by the cocrystallization process there are also bioavailability,[25−27] dissolution rate,[25,28−34] tabletability,[24,35] stability,[24,30−34,36−39]

Received: September 8, 2020
Revised: December 17, 2020
Published: December 28, 2020

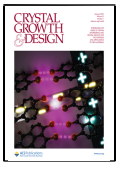

https://dx.doi.org/10.1021/acs.cgd.0c01242
Cryst. Growth Des. 2021, 21, 396−413

hygroscopicity,[38,40,41] flowability,[32,34,37,39] and mechanical properties.[33] One of the most important advantages of cocrystal formation is the possibility of modifying the physicochemical properties without changing or improving the pharmacological activity of the API and reducing side effects.[42,43]

We have used the following purine alkaloids as APIs for cocrystal formation. Caffeine, a popular substance with a psychoactive effect, affects the central nervous system, reduces fatigue, and increases concentration.[44−46] Theophylline is used primarily to treat acute asthma and chronic obstructive pulmonary disease.[47,48] Theobromine, in addition to acting on the human nervous system, according to Lee et al. also has anticarcinogenic activity (US Patent 2003/0099686A1).[49,50] The first two substances, namely caffeine and theophylline, are often used for cocrystallization with carboxylic acid derivatives.[51] They are readily soluble in water (theophylline 8.3 g L^{-1}, caffeine 16 g L^{-1}), but both of these alkaloids are easily converted from an anhydrous form to a hydrate.[48,52,53] In this case complex formation can affect both the solubility and the stability of these compounds in solution. Theobromine is less soluble in water (0.33 g L^{-1}) than theophylline and caffeine, and its cocrystallization can improve its solubility in water.[49]

1,3,5-Benzenetricarboxylic acid (trimesic acid) is a very popular coformer used for cocrystallization, inter alia with nitrogen aromatic bases, amines, carboxylic acids, alcohols, or neutral molecules such as alkenes and polycyclic aromatic hydrocarbons.[51] The choice of 1,2,3-benzenetricarboxylic acid (hemimellitic acid) was justified by its low popularity (five cocrystals and two salts in the CSD base).[51] The presented study of selected purine alkaloid cocrystals with the above carboxylic acids shows how difficult it is to predict the formation of specific supramolecular synthons in the designed structure. A better understanding of the self-assembly processes in systems containing many complex functional groups capable of forming noncovalent interactions is essential to enable complete control of the cocrystals design. This strategy is especially important when we think about pharmaceutical substances, because greater knowledge of the preferred supramolecular motifs in crystalline solids will allow better control of the properties of newly obtained multicomponent substances.[54]

2. EXPERIMENTAL SECTION

2.1. Materials. Theobromine, theophylline, and caffeine were purchased from Swiss Herbal Institute, Pol-Aura, and Coffeine Shop, respectively. Trimesic acid and hemimellitic acid were obtained from Sigma-Aldrich. All of the above substances were used without purification. Solvents were obtained from ChemPur. Millipore distilled water (18 MΩ) was used in all absorption experiments (Figure 1).

2.2. Solution-Based Cocrystallization. The selected purine alkaloid (theobromine, theophylline, or caffeine) and a given cocrystal former (trimesic or hemimellitic acid) were introduced to the selected solvent system in different stoichiometric ratios (Table S1). The mixtures were heated and stirred until the substances were completely dissolved. The cocrystals were obtained by slow evaporation from the filtrates under ambient conditions.

2.3. Mechanochemical Cocrystallization. The milling experiments were performed on a Retsch MM300 oscillatory ball mill. The stoichiometric ratios of the chosen purine alkaloid and coformer, together with two 4.0 mm stainless steel balls, were transferred into stainless steel jars. Grindings were carried out without (neat grinding) or in the presence of solvent (liquid-assisted grinding). Details of the milling conditions are presented in Table S2. Each experiment lasted 30 min at a frequency of 25 Hz.

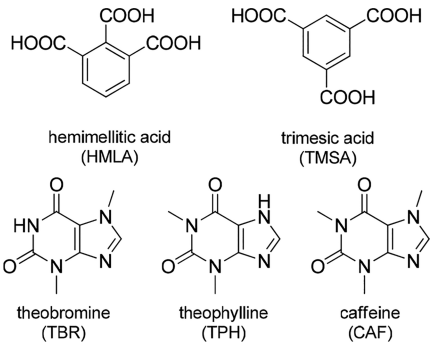

Figure 1. Structures of purine alkaloids and carboxylic acids used for cocrystallization.

2.4. Single-Crystal X-ray Diffraction (SXRD). Intensity data for all structures except $(TPH)^{+}\cdot(HMLA)^{-}\cdot 2H_2O$ were collected using an Oxford Diffraction SuperNova diffractometer with monochromatic Cu Kα radiation. Low temperatures (100−130 K) were achieved using the Cryojet cooling system. For $(TPH)^{+}\cdot(HMLA)^{-}\cdot 2H_2O$ data collection was performed at 100 K using a Rigaku XtaLAB Synergy-R diffractometer equipped with a rotating anode X-ray source (Cu Kα radiation) and a Cryostream cooling system. CrysAlis PRO was used for data collection and data reduction.[55] Crystal structures were solved using SHELXT-2015 (intrinsic phasing method) and refined using SHELXL-2015 (least-squares method).[56,57] The Olex2 program was used as an interface to structure solution and refinement.[58] The WinGX program was used for reflection data conversion into the HKLF5 format to refine two twinned structures.[59] The structural analysis was performed using Mercury.[60] In the investigated structures, except for CAF·TMSA, the difference Fourier map indicated the location of all hydrogen atoms. Details of the final treatment of hydrogen atoms, twin structures, disorders in crystal structures, and other restraints are presented in Table S3.

2.5. Powder X-ray Diffraction (PXRD). The X-ray diffraction patterns for cocrystals obtained by slow evaporation and grinding were collected on an Oxford Diffraction SuperNova diffractometer using Cu Kα radiation obtained at 50 kV and 0.8 mA. CrysAlis PRO was used for intensity data collection.[55] Samples were scanned between 5 and 40° (2θ) at a scanning step size of 0.01. All powder experiments were performed at room temperature. Theoretical diffractograms were generated using Mercury.[60] Powder patterns were processed using Kdif software.[61]

2.6. Solubility Measurements. The powdered samples of the obtained cocrystals were dissolved in Millipore distilled water (18 MΩ cm) and examined by using a Cary 100 (Agilent) dual-beam UV−vis spectrometer. UV−vis absorption spectra were recorded in the range of 200−800 nm with 1 nm increments. Quartz cells with 2 mm optical length were used. Standard curves of theobromine (Figure S19), theophylline (Figure S20), and caffeine (Figure S21) cocrystals were prepared. Substance concentrations versus absorbances of the substance at the detection wavelength (Table S4) were plotted. A linear relationship was obtained, and the slope was calculated from the graph. To determine the solubility of the cocrystals, saturated aqueous solutions of each were prepared. The absorbance at the detection wavelength (λ_{det}) was measured, and the concentration of the substance was determined using the Beer−Lambert equation. All experiments were repeated three times at room temperature, and the average of the results has been presented.

2.7. Hirshfeld Surface Analysis. The CrystalExplorer program was used to calculate molecular Hirshfeld surfaces for each component in all described complexes, except for water molecules.[62,63] The CIF files were imported into a program, and all bonds with hydrogen atom participation were modified into the values C−H = 1.083 Å, N−H = 1.009 Å, and O−H = 0.983 Å, which are standard neutron values. All surfaces were generated in standard (high)

https://dx.doi.org/10.1021/acs.cgd.0c01242
Cryst. Growth Des. 2021, 21, 396−413

resolution. The 2D fingerprint plots showing the interaction between different atoms and the intermolecular contacts are included in Table S9.1−8 and Figures S1−16 in the Supporting Information.

3. RESULTS AND DISCUSSION

Trimesic acid (TMSA) and hemimellitic acid (HMLA) were used for purine alkaloid cocrystallization: i.e., theobromine (TBR), theophylline (TPH), and caffeine (CAF). The crystallographic and refinement data are shown in Tables S5 and S6. All eight solids synthesized by solution-based and mechanochemical cocrystallizations were identified using the PXRD method. The SXRD measurements determined the structural characteristics and indication of individual supramolecular motifs. The difference Fourier map analysis, the C−O bond lengths in the carboxyl group involved in COOH···$N_{imidazole}$ formation, and the values of selected valence angles in the imidazole ring present in purine alkaloid molecules allowed the determination of the nature of the obtained compounds (cocrystal or salt) (Figure 2).

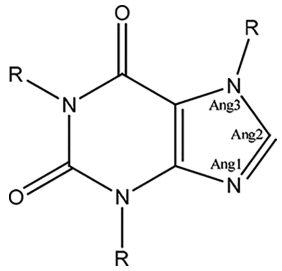

Figure 2. Selected bond angles for the analysis of the geometry of the imidazole ring in the neutral and cationic forms of purine alkaloid molecules.

Only the complex $(TPH)^{+}\cdot(HMLA)^{-}\cdot 2H_2O$ was identified as a salt. The peak on the difference Fourier map was positioned near the imidazole nitrogen atom. Additionally, the small difference between C═O and C−O bond distances (0.0429 Å) indicates a proton transfer and carboxylate anion formation (Table 1). The structures containing purine alkaloids in neutral and cationic form, where the proton was transferred to the imidazole nitrogen atom, were also analyzed for the imidazole ring geometry in the Cambridge Structural Database (ConQuest ver. 2.0.4, Table 2).[51,64] Values of specific valence angles in the imidazole ring of theophylline molecule in $(TPH)^{+}\cdot(HMLA)^{-}\cdot 2H_2O$ are in the range of angles corresponding to the protonated form of this purine alkaloid (Table 3). The calculated ΔpK_a value for this system (0.7, Table 4) is the highest of the calculated ΔpK_a values for all alkaloid−acid pairs described in this paper. This value is in the range from −1 to 4, where the probability of a obtaining salt increases with increasing ΔpK_a value, which is consistent with the obtained results.[65] An interesting fact is that for the same acid−base pair both the neutral complex TPH·HMLA and the ionic complex in the dihydrate form $(TPH)^{+}\cdot(HMLA)^{-}\cdot 2H_2O$ were obtained.

Table 1. Geometry of the Carboxyl Group Involved in COOH···$N_{imidazole}$ Formation

alkaloid−acid complex	$d_{C=O}$ (Å)	d_{C-O} (Å)	Δd (Å)
TBR·TMSA			
A[a]	1.215(3)	1.319(3)	0.104
B[a]	1.217(3)	1.315(3)	0.098
TPH·TMSA	1.216(2)	1.309(2)	0.093
TPH·TMSA·$2H_2O$[b]	1.2163(16)	1.3166(16)	0.1003
CAF·TMSA[c]	1.217(3)	1.319(3)	0.102
TBR·HMLA	1.202(3)	1.325(3)	0.123
TPH·HMLA	1.231(9)[d]	1.299(2)	0.068
$(TPH)^{+}\cdot(HMLA)^{-}\cdot 2H_2O$	1.2357(19)	1.2786(19)	0.0429
CAF·HMLA·H_2O	1.216(3)	1.303(3)	0.097

[a]Two theobromine molecules in the asymmetric unit of TBR·TMSA with A and B indices. [b]Data for the carboxyl group interacting with the imidazole nitrogen atom via the water molecule. [c]Data for the part of the structure with greater occupancy. [d]$d_{C=O}$ for the carbonyl oxygen atom with greater occupancy.

Table 2. Ranges of Bond Angles (deg) in the Imidazole Ring for Neutral and Protonated Forms of Alkaloid Molecules[a]

	neutral form of purine alkaloid molecules[b]	cationic form of purine alkaloid molecules[c]
Ang1	100.2−105.25	106.39−108.5
Ang2	111.41−117.0	108.89−111.44
Ang3	102.18−107.26	107.02−108.63

[a]Analysis based on data from Cambridge Structural Database using ConQuest[64] (search conditions: 3D coordinates determined, structure with $R \leq 0.075$, only single-crystal structures, only organic structures). [b]290 hits were found. [c]32 hits were found.

3.1. Synthesis Route. Theobromine cocrystals with both trimesic acid (TBR·TMSA) and hemimellitic acid (TBR·HMLA) were obtained by neat grinding. It was difficult to obtain the TPH·TMSA complex by milling without the addition of a solvent. The solution to this problem was adding a drop of methanol to the mixture of theophylline and acid to be ground. In turn, adding a drop of water to the same system produces TPH·TMSA·$2H_2O$ (Figure 3). Neat or liquid-assisted grinding with a drop of water of theophylline and hemimellitic acid always gives TPH·HMLA. The salt dihydrate $(TPH)^{+}\cdot(HMLA)^{-}\cdot 2H_2O$ could not be obtained by milling (Figure 4). The cocrystal CAF·TMSA and the cocrystal hydrate CAF·HMLA·H_2O were both obtained by neat grinding.

The above systems in Table 4 were obtained by slow evaporation from the solution. Information on the solvents used for crystallization can be found in Table S1 and in graphs with PXRD patterns (Figures 3 and 4). The challenge was to obtain the pure compound $(TPH)^{+}\cdot(HMLA)^{-}\cdot 2H_2O$. The anhydrous form TPH·HMLA was selectively obtained from a acetonitrile−water solution. Replacing acetonitrile with a different solvent (methanol, ethanol, isopropyl alcohol, *tert*-butyl alcohol) resulted mainly in the formation of an anhydrous form, which was confirmed by PXRD measurements; however, analysis of the crystals obtained from the above cocrystallizations under the microscope showed the presence of two forms. The use of a methanol−water mixture in several cases resulted in the pure dihydrate $(TPH)^{+}\cdot(HMLA)^{-}\cdot 2H_2O$. Two out of the nine powder patterns in Figure 4.3 show that cocrystallization from methanol−water can lead to both the anhydrous and hydrated forms.

3.2. Crystal Structure Analysis. *3.2.1. Theobromine Benzene-1,3,5-tricarboxylic Acid Cocrystal (TBR·TMSA).* Theobromine and trimesic acid cocrystallize in the monoclinic space group $P2_1/c$ with $Z' = 2$ (Figure 5a). The asymmetric unit contains two TBR and two TMSA molecules.

https://dx.doi.org/10.1021/acs.cgd.0c01242
Cryst. Growth Des. 2021, 21, 396−413

Table 3. Imidazole Ring Geometry: Bond Angles (deg) for the Structures Described in This Paper

cocrystal	Ang1	Ang2	Ang3
TBR·TMSA (A molecule)	104.5(2)	113.1(2)	106.1(2)
TBR·TMSA (B molecule)	104.1(2)	113.0(2)	106.2(2)
TPH·TMSA	104.6(1)	112.3(1)	106.9(1)
TPH·TMSA·2H_2O	103.5(1)	113.6(1)	106.1(1)
CAF·TMSA (89% occupancy)	104.0(2)	112.9(2)	106.1(2)
CAF·TMSA (11% occupancy)	104(2)	114(2)	107.8(2)
TBR·HMLA	103.6(2)	113.7(2)	105.8(2)
TPH·HMLA	104.1(1)	112.6(1)	106.8(1)
$(TPH)^+\cdot(HMLA)^-\cdot 2H_2O$	106.26(12)	111.30(13)	107.32(12)
CAF·HMLA·H_2O	104.1(2)	113.0(2)	106.0(2)

Table 4. Calculated ΔpK_a Values for All Alkaloid–Acid Pairs

alkaloid–acid pair	pK_a of protonated alkaloid[66,67]	pK_a of acid (pK_{a_1} value)[68]	ΔpK_a = pK_a(protonated base) − pK_a(acid)[65]
TBR–TMSA	0.12	3.12	−3.0
TBR–HMLA	0.12	2.80	−2.68
CAF–TMSA	0.6	3.12	−2.52
CAF–HMLA	0.6	2.80	−2.20
TPH–TMSA	3.5	3.12	0.38
TPH–HMLA	3.5	2.80	0.7

Components of this cocrystal form layers parallel to the (101) crystallographic plane (Figure 5b). Within these layers, chains of carboxylic acids connected by O6A–H6A···O3B and O6B–H6B···O3A hydrogen bonds can be observed. Between these chains, theobromine molecules create amide–amide dimers $R_2^2(8)$ via N1A–H1A···O8B and N1B–H1B···O8A interactions with *endo*-carbonyl oxygen atom participation. Each alkaloid molecule is connected to two trimesic acid molecules. Typical COOH···$N_{imidazole}$ heterosynthons were formed (O2A–H2A···N4A and O2B–H2B···N4B hydrogen bonds, Table S8). The *exo*-carbonyl oxygen atoms in purine alkaloid

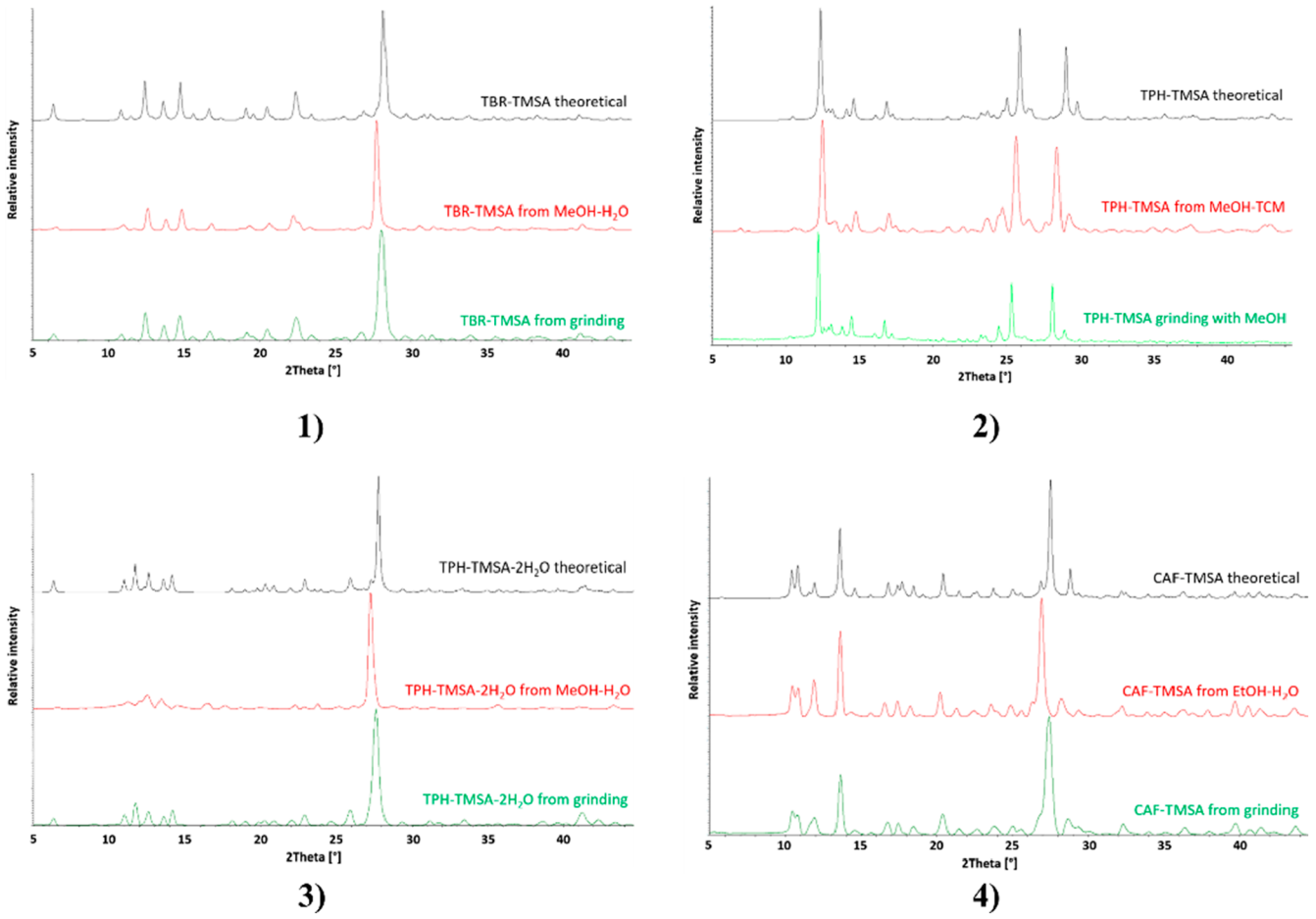

Figure 3. PXRD patterns of the cocrystals with trimesic acid as the coformer: (1) theobromine trimesic acid cocrystal; (2) theophylline trimesic acid cocrystal; (3) theophylline trimesic acid dihydrate; (4) caffeine trimesic acid cocrystal Color code: black, theoretical pattern; red, powder pattern for sample obtained by slow evaporation from solution; green, powder pattern for sample from grinding.

https://dx.doi.org/10.1021/acs.cgd.0c01242
Cryst. Growth Des. 2021, 21, 396–413

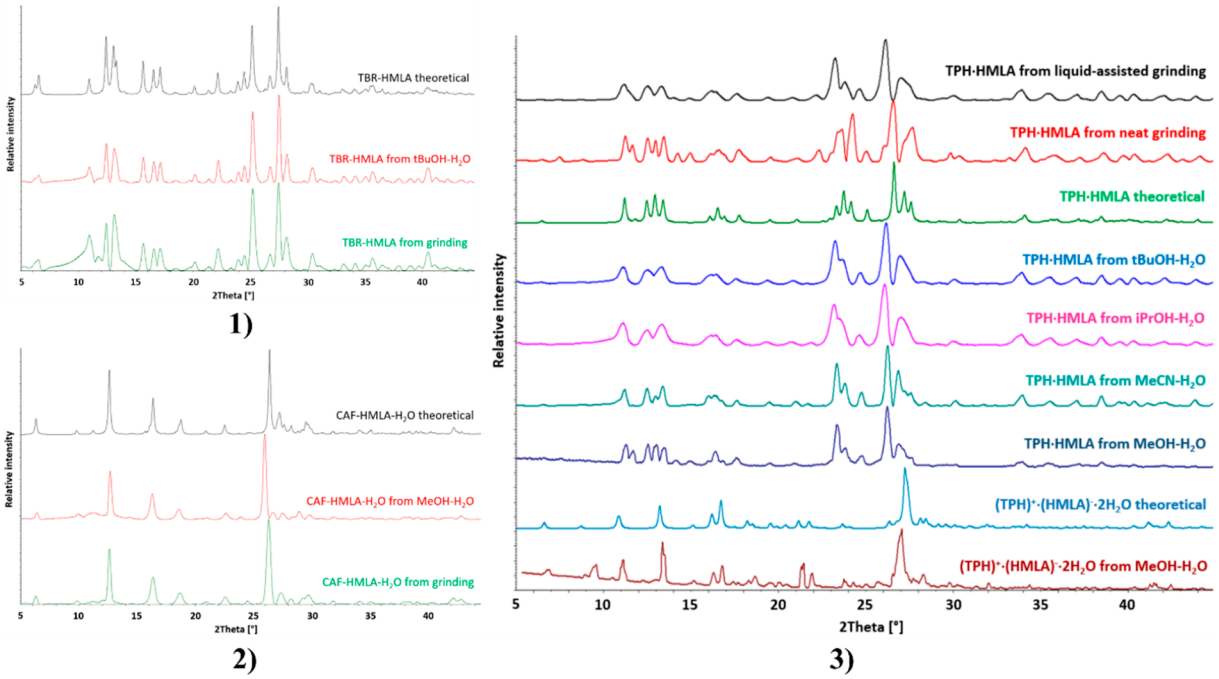

Figure 4. PXRD patterns of the alkaloid systems with hemimellitic acid as coformer: (1) theobromine hemimellitic acid cocrystal; (2) caffeine hemimellitic acid monohydrate; (3) theophylline with hemimellitic acid, cocrystal and salt dihydrate.

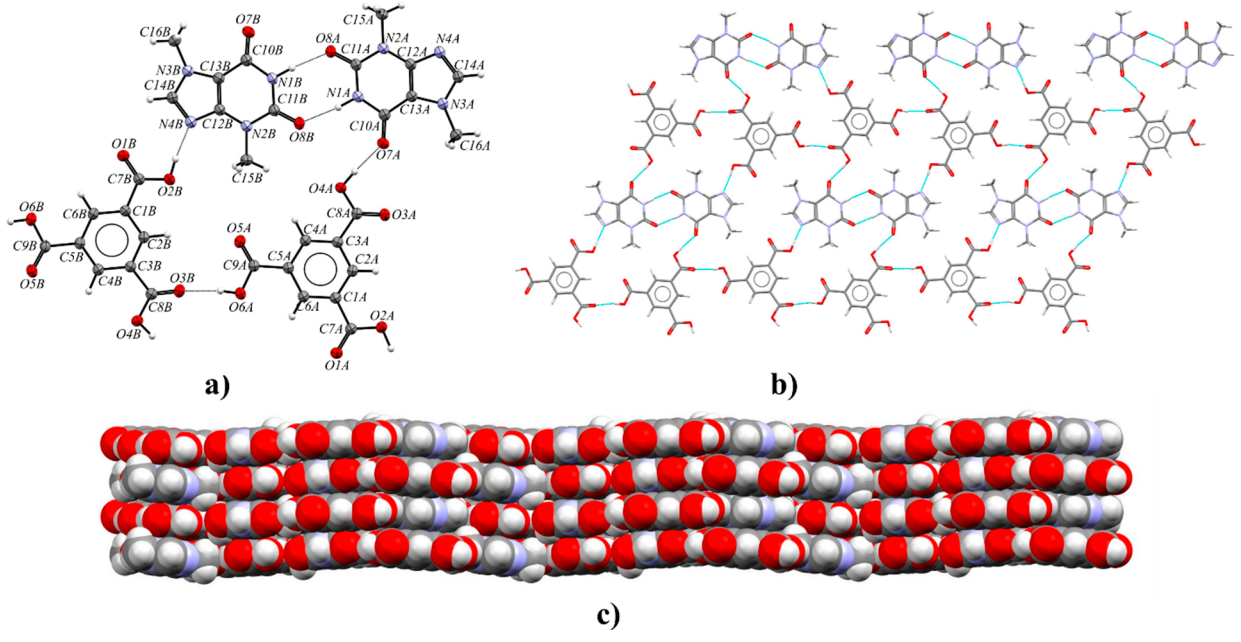

Figure 5. (a) ORTEP representation of the TBR·TMSA asymmetric unit (thermal ellipsoids were plotted at the 50% probability level). (b) 2D structure showing a molecular layer, with a projection on the (101) crystallographic plane. (c) 3D structure of the TBR·TMSA stabilized by $\pi\cdots\pi$ forces, in a view along the $[10\bar{1}]$ direction.

molecules (O7A and O7B) are proton acceptors from carboxylic groups (O4A−H4A···O7A and O4B−H4B···O7B hydrogen bonds). These layers form a 3D network through the π(TBR)···π(TMSA) forces (Figure 5c and Table S7).

*3.2.2. Theophylline Benzene-1,3,5-tricarboxylic Acid Cocrystal (**TPH·TMSA**).* Theophylline and trimesic acid form a cocrystal in the monoclinic space group $P2_1/c$ with one alkaloid and one acid molecule in the asymmetric unit (Figure 6a). TMSA molecules are hydrogen-bonded with two neighboring acids via O4−H4···O1 interactions (Table S8). In this way, an infinite helical system $C_2^2(16)$ around the 2_1 screw axis parallel to the [010] direction is formed. The pitch of the helix is 13.4344(2) Å with two acid molecules per turn (Figure 6b). Alkaloid molecules are connected with two benzene-1,3,5-tricarboxylic acid molecules. Theophylline with one acid molecule forms a COOH···$N_{imidazole}$ synthon (O2−H2···N4 hydrogen bond). The heterosynthon TPH-ACID $R_2^2(9)$ is formed through O6−H6···O7 and N3−H3···O5 hydrogen bonds. Neighboring helical systems are interdigitated

https://dx.doi.org/10.1021/acs.cgd.0c01242
Cryst. Growth Des. 2021, 21, 396−413

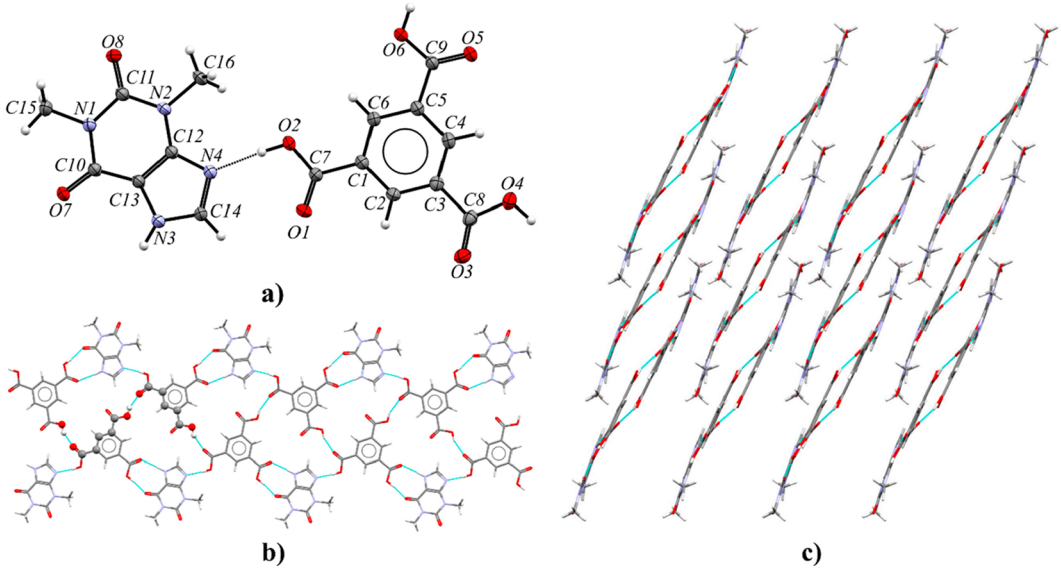

Figure 6. (a) ORTEP view of the TPH·TMSA asymmetric unit (displacement ellipsoids plotted at the 50% probability level; disordered fragments in TPH molecule are omitted for clarity). (b) Helix arrangement around the screw axis 2_1 parallel to the [010] direction, in a view along the [405] direction. (c) 3D structure composed of interconnected helical systems via C−H···O and $\pi\cdots\pi$ interactions, in a view along the [010] direction.

by C−H···O forces between theophylline molecules and by π(TPH)···π(TMSA) interactions (Figure 6c and Table S7).

3.2.3. Theophylline Benzene-1,3,5-tricarboxylic Acid Dihydrate (TPH·TMSA·2H$_2$O). Theophylline and trimesic acid can form a cocrystal hydrate in the triclinic space group $P\bar{1}$. The asymmetric unit consists of one alkaloid, one acid, and two water molecules (Figure 7a). Components of this solid are arranged in layers parallel to the (213) crystallographic plane (Figure 7b). In the crystal lattice, TMSA molecules form $R_2^2(8)$ homosynthons through O−H···O (O3−H3A···O4 and O4−H4···O3, Table S8) hydrogen bonds. The hydrogen atoms H3A and H4 in TMSA carboxyl groups, involved in acid−acid synthon formation, are disordered with occupancies 0.45:0.55. The $R_2^2(9)$ theophylline−acid heterosynthons are sustained by N3−H3···O5 and O6−H6···O7 interactions. In both solvent molecules, one of the hydrogen atoms is disordered over two positions with 0.50 occupancies (H9B, H9C and H10A, H10C atoms). The hydrogen bonds with the participation of these hydrogen atoms (O9−H9B···O9, O9−H9C···O10, O10−H10A···O9, O10−H10C···O10, Table S8) are responsible for the connection of the water molecules, resulting in an infinite channel formation parallel to the [100] direction (Figure 7c). The ordered hydrogen atoms are noncovalently bonded to the carbonyl group (O10−H10B···O1 hydrogen bond) and the imidazole nitrogen atom of theophylline (O9−H9A···N4 hydrogen bond), respectively. The last interaction and the O2−H2···O9 hydrogen bond are an interesting case, where one water molecule bridges the carboxylic acid and imidazole functionalities of the expected COOH···N$_{imidazole}$ heterosynthon (a so-called "masked synthon").[69] The 3D stacks are also stabilized by π(TPH)···π(TMSA) and C−H···O forces (Figure 7d and Table S7).

The presented complex was also obtained by Abosede et al., but some structural differences are observed.[70] Oxygen atoms of water molecules in the described TPH·TMSA·2H$_2$O crystal structure are ordered. In both solvent molecules, one hydrogen atom is ordered, whereas the second hydrogen atom is disordered equally over the two sites. Channels of hydrogen-bonded water molecules along the [100] direction are observed. In the deposited structure (refcode HUHQIN), one of the hydrogen atoms in one of the water molecules is disordered over two positions, but in the second water molecule an oxygen atom is disordered over two positions with occupancies 0.94:0.06, where hydrogen atoms in the solvent molecule with smaller occupancy were not identified. Moreover, in contrast to the already published structure, in the carboxyl groups involved in acid−acid dimer formation, a disorder of a hydrogen atom over two sites with occupancies 0.45:0.55 can be observed. The measurement of TPH·TMSA·2H$_2$O at 130 K made it possible to precisely determine the position of all hydrogen atoms from the difference Fourier map and to identify disordered atoms.

3.2.4. Caffeine Benzene-1,3,5-tricarboxylic Acid Cocrystal (CAF·TMSA). The caffeine−benzene-1,3,5-tricarboxylic acid cocrystal crystallizes in the *Pbca* space group with one CAF and one TMSA molecule in the asymmetric unit (Figure 8a). The purine alkaloid and half of the acid molecule are disordered over two sites with occupancies 0.89:0.11 (Figure 8b). Figure 8d shows the disorder in a larger structural fragment. The superimposition of more and less occupied fragments indicates the structural disorder by the mirror plane (the RMS deviation index is equal to about 0.15). However, the CAF·TMSA structure obtained and described by Abosede et al. is completely ordered (refcode HUHQUZ).[70] Each CAF molecule is hydrogen-bonded to one acid molecule via a O2−H2···N4 interaction (or O2A−H2A···N4A, Table S8). The remaining two carboxyl groups form $R_2^2(8)$ homodimers sustained by O4−H4···O5 and O6−H6···O3 hydrogen bonds with neighboring acid molecules. In this way, zigzag-shaped polymer chains along the 2_1 axis parallel to the [010] direction are formed (Figure 8c). The C−H···O and $\pi\cdots\pi$ forces between caffeine molecules are responsible for the 3D network formation and stabilization (Figure 8e and Table S7).

3.2.5. Theobromine Benzene-1,2,3-tricarboxylic Acid Cocrystal (TBR·HMLA). Theobromine and hemimellitic acid cocrystallize in a 1:1 stoichiometric ratio in the monoclinic space group *C*2/*c* (Figure 9a). Components of this cocrystal form wavelike chains through O4−H4···N4 interactions

https://dx.doi.org/10.1021/acs.cgd.0c01242
Cryst. Growth Des. 2021, 21, 396−413

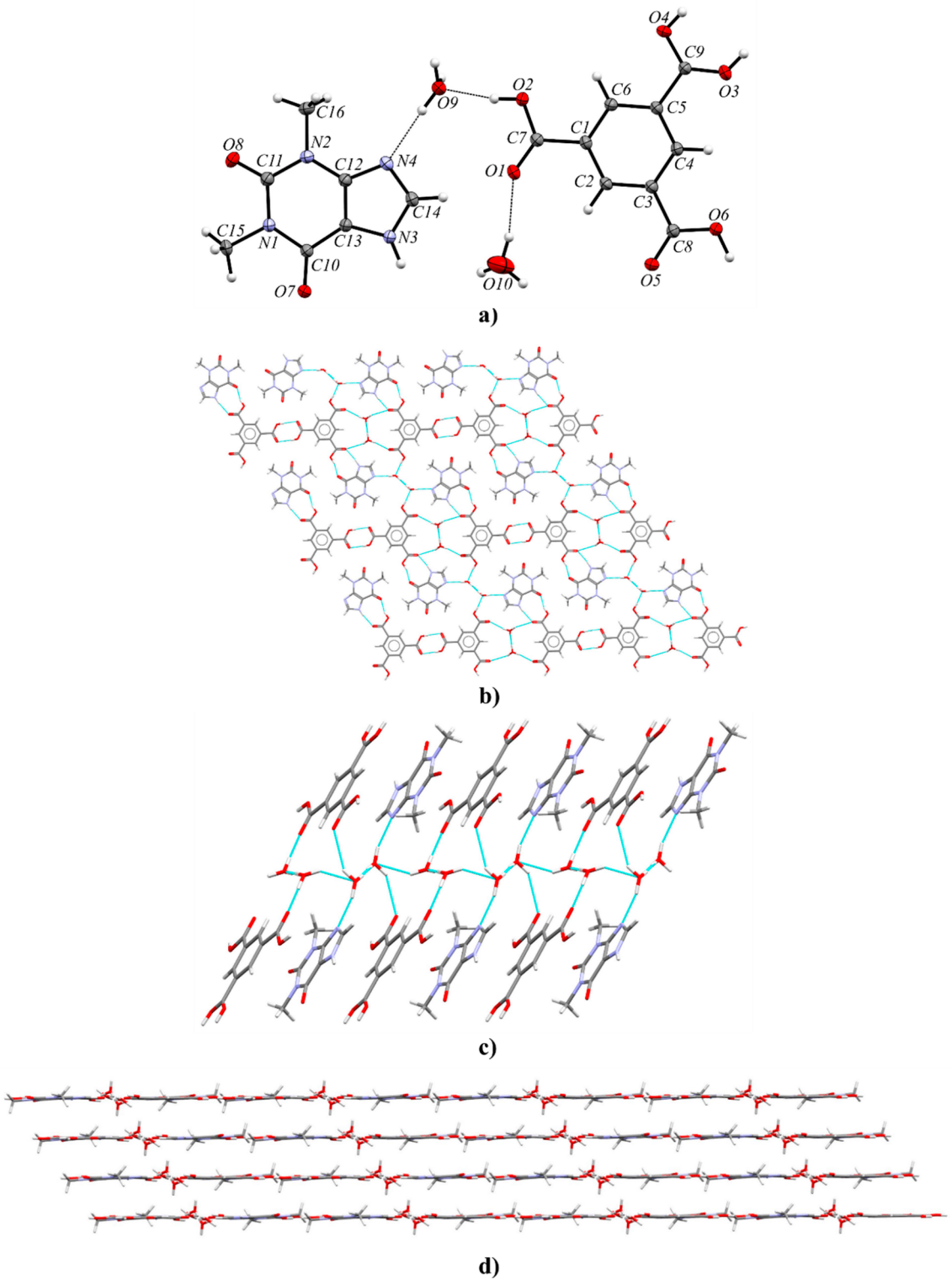

Figure 7. (a) ORTEP representation showing the asymmetric unit of TPH·TMSA·2H_2O with numbering of atoms (thermal ellipsoids were drawn at the 50% probability level, both water molecules are disordered, the hydrogen atom near the carboxyl group with the C9 atom is disordered over two sites with occupancies 0.55:0.45, and rotational disorder of the C16 methyl group is not presented for clarity);. (b) 2D molecular layer parallel to the (213) plane, in a projection on the (213) crystallographic plane (disorder in the C16 methyl group and in the carboxyl group is omitted for clarity). (c) Channel of hydrogen-bonded water molecules running along the [100] direction, in a view along the [$2\bar{4}1$] direction. (d) 3D layered structure, in a view along the [$1\bar{2}0$] direction.

(COOH···$N_{imidazole}$ synthon) and $R_2^2(8)$ cyclic motifs composed of O2−H2···O7 and N1−H1···O1 hydrogen bonds (Figure 9c and Table S8). Two of these zigzag ribbons are interconnected through carboxylic acid homodimer formation (O6−H6···O6 or O6A−H6A···O6A hydrogen bond) between two HMLA molecules (Figure 9b). This dual system along the [$10\bar{1}$] crystallographic direction (Figure 9c) is also stabilized by C−H···O and π(TBR)···π(TBR) interactions. Acid−acid

https://dx.doi.org/10.1021/acs.cgd.0c01242
Cryst. Growth Des. 2021, 21, 396−413

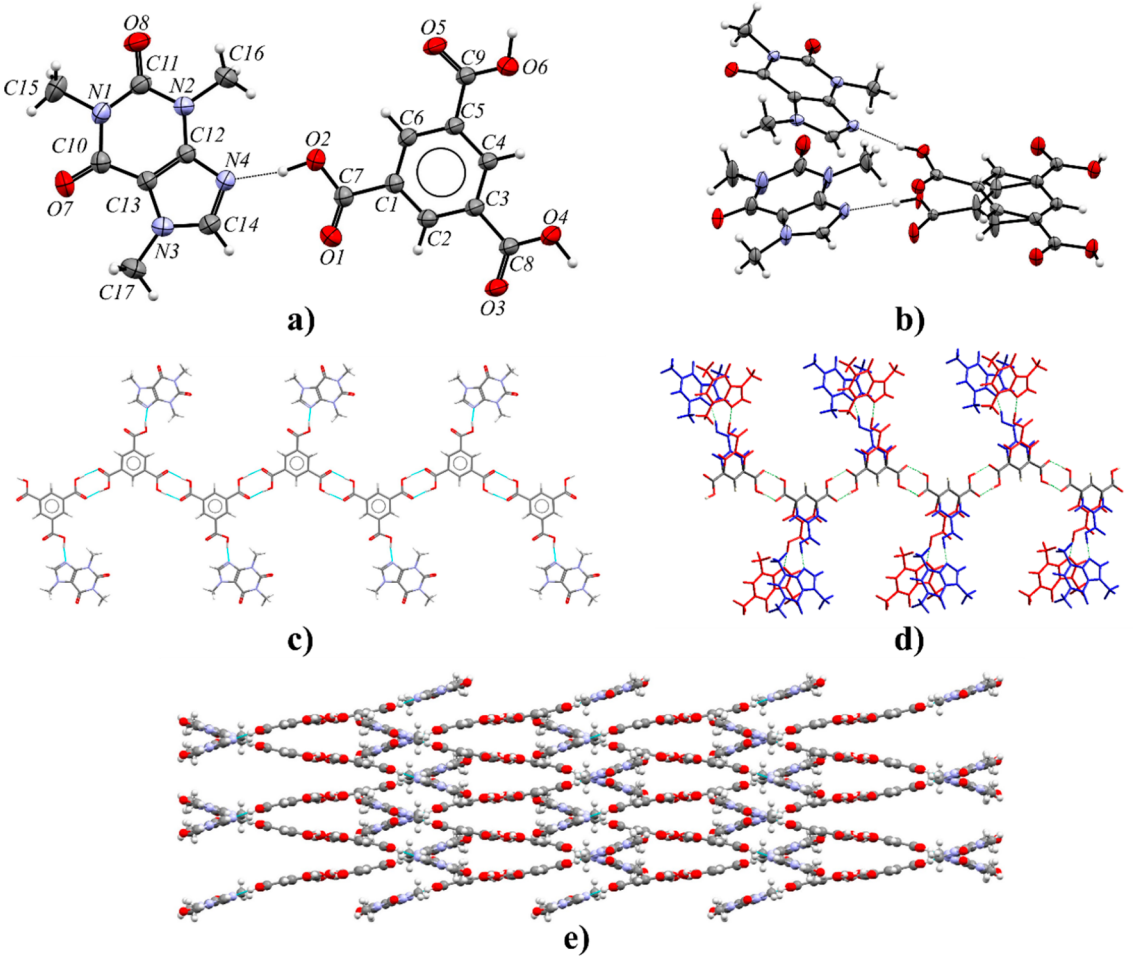

Figure 8. (a) ORTEP representation of the CAF·TMSA asymmetric unit (the highest occupancy is presented). (b) ORTEP representation of the more (top part) and less occupied fragments (bottom part) of the CAF·TMSA asymmetric unit (thermal ellipsoids plotted at the 50% probability level). (c) 1D polymer zigzag chain parallel to screw axis 2_1 along the [010] direction consisting of CAF and TMSA molecules with the highest occupancy, in a view along the [100] direction. (d) Zigzag polymer disorder in the CAF·TMSA crystal lattice (blue, greater occupancy 0.89; red, smaller occupancy 0.11). (e) crystal packing of CAF·TMSA showing interdigitated zigzag polymers, in a view along the [010] direction.

homodimers are formed around the C_2 axis. A small difference in C−O bond lengths (1.242(3) Å for C9−O5 and 1.238(4) Å for C9−O6) in the carboxyl group involved in the formation of these dimers shows that this group is affected by the disorder. The introduction of a hydrogen atom disorder model in this carboxyl group does not solve the C−O bond length problem. Only the disorder of the carboxyl group by rotation around the C3−C9 bond solved the above problem. After this procedure, the C−O bond lengths indicated the single and double bond sites as well as proton locations. In the final model, this group is disordered over two positions with fixed occupancies equal to 50%. The 3D network is sustained by π(TBR)···π(TBR) and π(HMLA)···π(HMLA) interactions between the neighboring chains (Figure 9d and Table S8).

3.2.6. Theophylline Benzene-1,2,3-tricarboxylic Acid Cocrystal (TPH·HMLA). Theophylline and benzene-1,2,3-tricarboxylic acid cocrystallize in the triclinic space group $P\bar{1}$ with $Z' = 1$ (Figure 10a). Each TPH molecule is noncovalently connected with three HMLA molecules and one HMLA molecule with three TPH molecules (Figure 10b). In the crystal lattice, centrosymmetric four-component aggregates are recognized, which are sustained via O2−H2···N4 (COOH···$N_{imidazole}$) and O4−H4···O8 hydrogen bonds (Table S8). These systems within the 1D molecular ribbon are held together by $R_2^2(9)$ cyclic arrays of N3−H3···O5 and O6−H6···O7 interactions. The ribbons connected through π(TPH)···π(HMLA) and C−H···O forces form a three-dimensional structure (Figure 10c and Table S7).

3.2.7. Theophyllinium 2,6-Dicarboxybenzoate Dihydrate $(TPH)^+\cdot(HMLA)^-\cdot 2H_2O$. Theophylline and benzene-1,2,3-tricarboxylic acid form a salt hydrate with two cocrystallized water molecules in the monoclinic $I2/a$ space group (Figure 11a). The crystals of this compound exhibit nonmerohedral twinning. The components in the crystal lattice of $(TPH)^+\cdot(HMLA)^-\cdot 2H_2O$ form a complex system of strong hydrogen bonds. The carboxyl group in the 2,6-dicarboxybenzoate anion near the C1 atom, theophyllinium cation, and water molecule (with disordered O9 atom) are involved in the 10-membered hydrogen-bonded ring formation through O2−H2···O7, N3−H3···O9 (or N3−H3···O9A), and O9−H9B···O1 (or O9A−H9B···O1) interactions (Figure 11c and Table S8). This water molecule donates a proton to the carbonyl oxygen atom (O9−H9A···O3 or O9A−H9A···O3 hydrogen bond) in the carboxylate ion of HMLA. A proton transfer from this group to the imidazole nitrogen atom of theophylline was observed (N4−H4···O4 interaction, Figure 11a). The third carboxyl group is a proton donor to the O10 oxygen atom in an ordered water molecule (O6−H6···O10 hydrogen bond). The

https://dx.doi.org/10.1021/acs.cgd.0c01242
Cryst. Growth Des. 2021, 21, 396−413

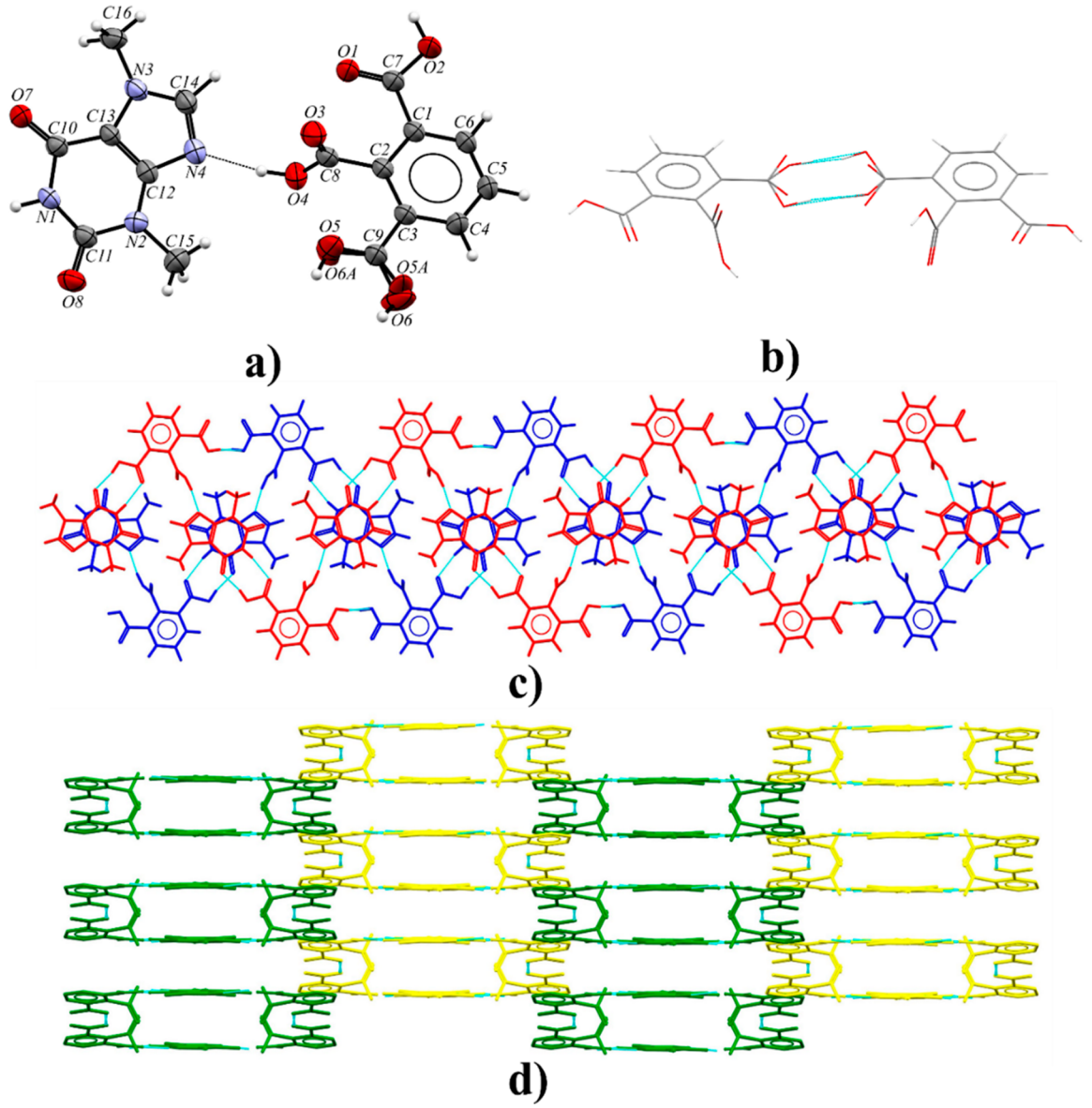

Figure 9. (a) ORTEP representation showing the asymmetric unit of the TBR·HMLA (the rotational disorder of the carboxyl group in HMLA near the C9 atom is shown, and the disorder of both methyl groups in TBR are omitted for clarity; displacement ellipsoids are drawn at the 50% probability level). (b) Representation of the acid−acid dimer formed around the C_2 axis with disordered carboxyl groups. (c) One-dimensional structural motif composed of two wavelike chains through $[10\bar{1}]$ direction, in a view along the [104] direction; (d) 3D crystal structure of TBR·HMLA stabilized by $\pi\cdots\pi$ interactions, in a view along the $[10\bar{1}]$ direction.

molecular chains along the [100] direction are formed by noncovalent O10−H10A···O4 and O10−H10B···O3 interactions between ordered solvent molecules and the oxygen atoms of the internal $-COO^-$ groups of the acid anion (Figure 11b and Table S8). The three-dimensional crystal structure is also stabilized by C−H···O and π(TPH)···π(TPH) forces (Table S7).

3.2.8. Caffeine Benzene-1,2,3-tricarboxylic Acid Monohydrate (CAF·HMLA·H_2O). Caffeine hemimellitic acid monohydrate crystallizes in the monoclinic $P2_1/c$ space group (Figure 12a). The alkaloid molecules are hydrogen-bonded via O4−H4···N4 interactions with the internal acidic groups of HMLA (COOH···$N_{imidazole}$ synthon, Table S8). Two outer carboxyl groups of two HMLA molecules together with a water molecule are involved in $R_3^3(10)$ ring formation (Figure 12b). The O2−H2···O5 hydrogen bond is a direct contact between carboxyl groups. The modification in the acid−acid dimer formation by incorporation of water molecules is observed; thus, "moderate synthons" are formed.[69] The solvent molecules, noncovalently bonded with three acid molecules by O9−H9A···O1, O9−H9B···O3, and O6−H6···O9 interactions, are responsible for a double-molecular-ribbon formation. These motifs run along the 2_1 axes at the 1/2, *y*, 1/4 and 1/2, *y*, 3/4 positions, and they are interconnected by C−H···O and C−H···π interactions to form the 3D crystal structure (Figure 12c).

3.3. Supramolecular Analysis of Novel Alkaloid−Acid Compounds. Theobromine, theophylline, and caffeine were chosen for cocrystallization with both trimesic and hemimellitic acids. Purine alkaloids differ in the number and location of methyl groups. The benzene-1,3,5-tricarboxylic acid molecule is flat, while in the benzene-1,2,3-tricarboxylic acid

https://dx.doi.org/10.1021/acs.cgd.0c01242
Cryst. Growth Des. 2021, 21, 396−413

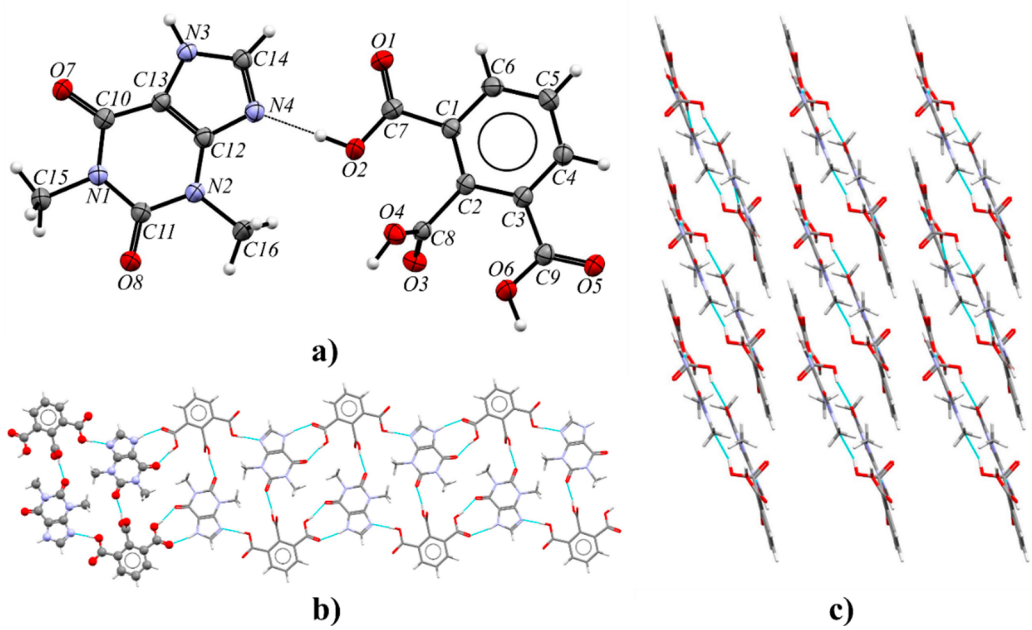

Figure 10. (a) ORTEP representation of the TPH·HMLA asymmetric unit with the atomic numbering scheme (the disorder of the O1 carbonyl atom is omitted for clarity; thermal ellipsoids are plotted at the 50% probability level). (b) 1D molecular ribbon composed of four-component aggregates along the [001] direction, in a view along the [4$\bar{1}$0] direction. (c) 3D structure showing adjacent ribbons of TPH·HMLA, in a view along the [001] direction.

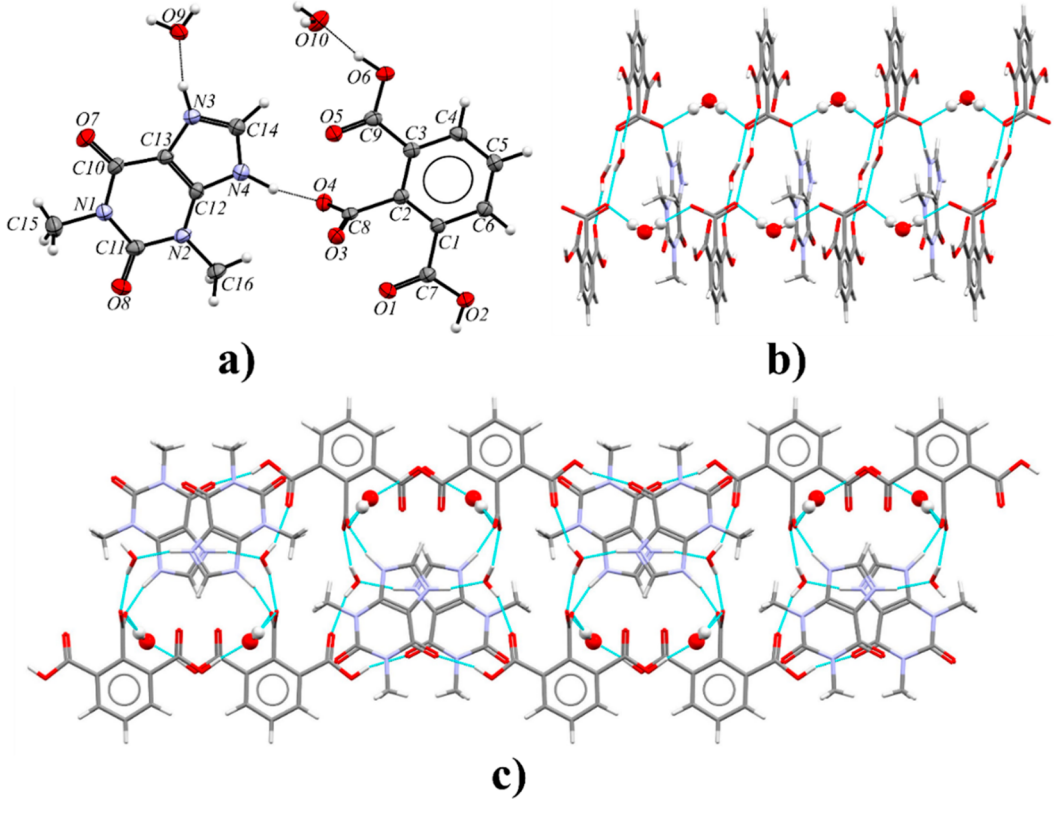

Figure 11. (a) ORTEP representation of the $(TPH)^{+}\cdot(HMLA)^{-}\cdot 2H_2O$ asymmetric unit (disordered fragments are not presented for clarity; thermal ellipsoids are drawn at the 50% probability level). (b) Molecular chains along the [100] direction formed as a result of noncovalent bonding of water molecules (the O10 atom, presented in ball and stick form) and carboxylate groups, in a view along the [$\bar{2}$30] direction. (c) 2D structure of $(TPH)^{+}\cdot(HMLA)^{-}\cdot 2H_2O$, in a view along the [100] direction.

molecule, the proximity of carboxyl groups makes the internal carboxyl group twisted with respect to the aromatic ring (Table 5).

Therefore, the carboxyl group positions in the studied coformer molecules certainly affect the number of possible noncovalent connections between molecules. Selected co-

https://dx.doi.org/10.1021/acs.cgd.0c01242
Cryst. Growth Des. 2021, 21, 396−413

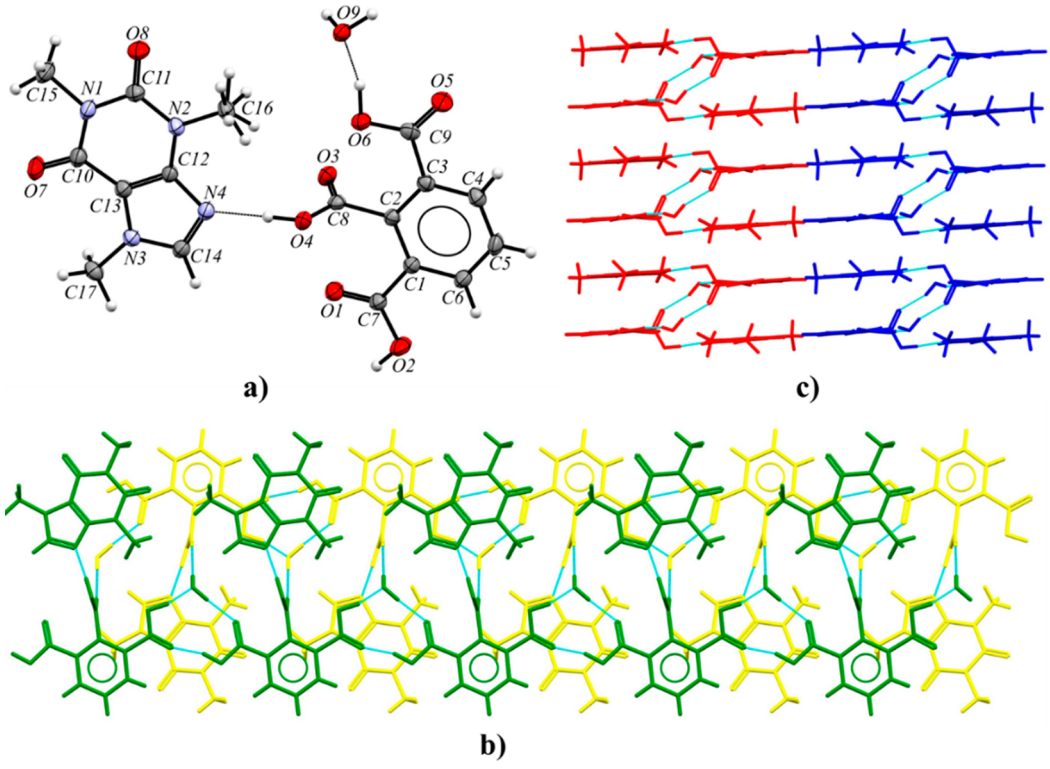

Figure 12. (a) ORTEP representation of the CAF·HMLA·H_2O asymmetric unit with a disordered methyl group of caffeine (displacement ellipsoids are drawn at the 50% probability level). (b) Double ribbon along the 2_1 screw axis parallel to the [010] direction, in a view along the [100] direction. (c) 3D structure of CAF·HMLA·H_2O stabilized by C−H···O and C−H···π interactions, in a view along the [010] direction.

Table 5. Geometry of the Internal Carboxyl Group of Hemimellitic Acid in Its Complexes, Defined as the Torsion Angle at Which the Internal Group in This Acid Is Twisted Relative to the Benzene Ring

alkaloid−HMLA complex	internal group orientation (deg)
TBR·HMLA	97.3(3)
TPH·HMLA	99.84(16)
$(TPH)^+\cdot(HMLA)^-\cdot 2H_2O$	83.14(17)
CAF·HMLA·H_2O	84.1(3)

formers can form strong hydrogen bonds only with carboxyl groups; thus, we can distinguish three types of supramolecular synthons at the cocrystal design stage: alkaloid−alkaloid (amide−amide, Figure 13.1), alkaloid−acid (amide−acid, Figure 13.2), and acid−acid (Figure 13.3) synthons. The structural studies for the described compounds confirmed the dominant role of alkaloid−acid and acid−acid synthons in comparison with alkaloid−alkaloid homosynthons, due to the dominant amount of carboxyl acid groups in the coformer molecules.

3.3.1. Theobromine Derivatives. Theobromine forms cocrystals with both trimesic and hemimellitic acids. Among the eight compounds described in this paper, only in TBR·TMSA cocrystal was an alkaloid−alkaloid synthon type observed. TBR-TBR dimers (homosynthon II) connected by weak interactions are present in the crystal lattice of pure theobromine (Figure 13.1b).[72] This type of homosynthon is also found in only one TBR−acid system, where 4-hydroxybenzoic acid was used as a coformer.[73] The formation of a TBR−TBR homosynthon I in the presence of a carboxyl group is more favored than homosynthon II.[51,74] Surprisingly, in the presence of TMSA the TBR−TBR homosynthon II is still observed (Figure 13.1b). The acid molecules joined noncovalently with alkaloid molecules through COOH···$N_{imidazole}$ hydrogen bonds (Figure 13.2g) and with the carbonyl oxygen atom near the pyrimidine ring, which do not participate in the TBR−TBR homosynthon formation (Figure 14a, TBR−acid homosynthon III). The acid molecules are interconnected via O−H···O interactions by heterodimer formation (Figure 13.3b). Carboxylic acids can also form infinite chains, so-called catemers, in which one carboxyl group is bonded noncovalently to two different adjacent groups. This motif is rarely observed: i.e., in acemetacin, tetrolic acid, and 2,6-bis(trifluoromethyl)benzoic acid. It is also not observed in our structures.[75−77]

On the other hand, the use of hemimellitic acid resulted in breaking the N−H···O hydrogen bonds between theobromine molecules and forming the TBR−acid heterosynton I (external carboxyl group of acid), and the second carbonyl oxygen atom did not participate in strong interactions (Figure 13.2a). In the COOH···$N_{imidazole}$ hydrogen bond formation, the internal carboxyl group is involved. It was unexpected to identify an acid−acid dimer (hydroxyl dimer, Figure 14b), in which only hydroxyl groups are responsible for the strong interactions between these groups (they act as both hydrogen bond donors and acceptors). In the 140 crystal structures found in the CSD base, this type of dimer was identified.[51] The same synthon with carbonyl oxygen atoms on the same side is present in 56 structures. In 32 structures, this dimer was formed around the C_2 axis, and 10 of them crystallize in the $C2/c$ space group, similarly to the theobromine hemimellitic acid cocrystal.

3.3.2. Theophylline Derivatives. Theophylline with trimesic acid forms both a cocrystal and a cocrystal hydrate. Only three organic acids were found in the CSD base that in combination

https://dx.doi.org/10.1021/acs.cgd.0c01242
Cryst. Growth Des. 2021, 21, 396−413

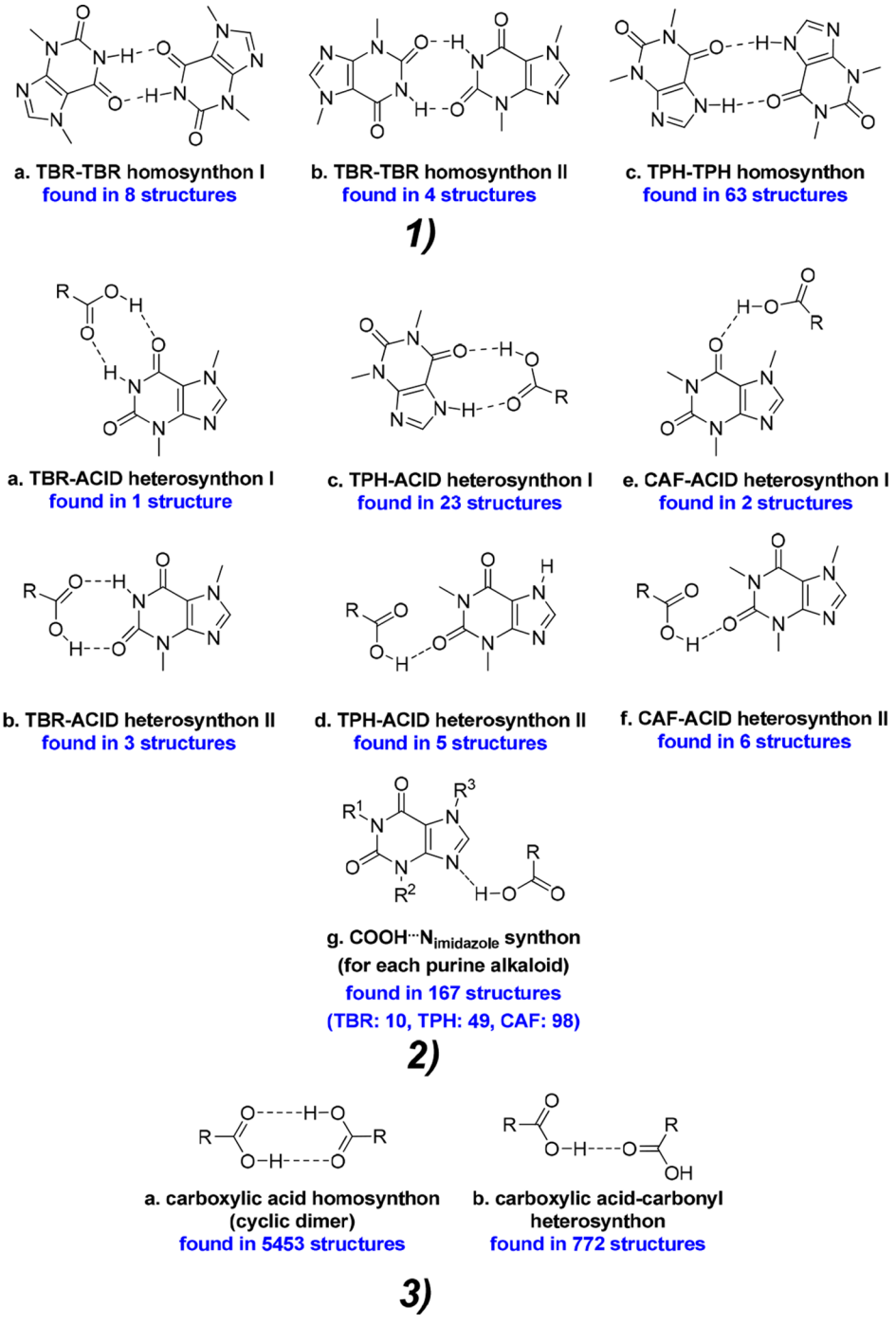

Figure 13. (1) Typical alkaloid−alkaloid synthons observed in the crystal structures of alkaloid−carboxylic acid complexes. (2) The most frequently observed alkaloid−acid heterosynthons observed in alkaloid−acid systems. (3) The two most common types of carboxylic acid dimers in crystal structures.[71] The number of structures found in the CSD base with a given synthon is given in blue (Search conditions: 3D coordinates determined, structure with $R \leq 0.1$, no errors, only organic structures. An additional condition for carboxylic acid synthons was "normalize terminal H positions").

with TPH have both forms (Table 6).[51] In both structures, TPH−TPH homosynthons (Figure 13.1c) are not observed, as expected, due to the presence of several carboxyl groups in the coformer molecules. TPH−acid heterosynthon I was formed in both anhydrous and dihydrate crystals (Figure 13.2c). In the TPH·TMSA cocrystal, the most expected COOH···$N_{imidazole}$ synthon is observed (Figure 13.2 g). In TPH·TMSA·$2H_2O$, a water molecule bridges the imidazole to carboxyl interaction (Figure 15a). This type of synthon was found only in two structures (REFCOD: KIGKAN, KIKHUI).[51] In the anhydrous complex, the dimers between carboxyl groups through O−H(carboxyl)···O═C(carboxyl) interactions are formed (Figure 13.3b). The inclusion of water molecules in the crystal lattice results in the cyclic acid−acid dimer formation (Figure 13.3a).

Theophylline and hemimellitic acid formed unexpectedly two types of complexes—the neutral TPH·HMLA and proton-transfer complex $(TPH)^{+}\cdot(HMLA)^{-}\cdot 2H_2O$. Homosynthons

https://dx.doi.org/10.1021/acs.cgd.0c01242
Cryst. Growth Des. 2021, 21, 396−413

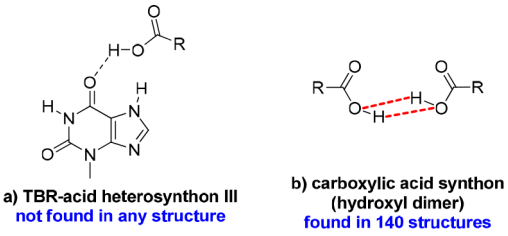

Figure 14. Additional synthons identified in the described theobromine cocrystals. The dashed red bonds show the hydrogen bonds between hydroxyl groups.

Table 6. Coformers That Form Anhydrous and Hydrate Forms of Cocrystals with Theophylline

coformer	pK_a value of coformer	anhydrous form[a]	hydrate form[b]
anthranilic acid	2.108	2:3[78]	3:2:4 and 2:1:4[78]
2,4-dihydroxybenzoic acid	3.32	1:1[79]	1:1:1[80]
citric acid	3.15	1:1[c,81]	1:1:1[81]

[a]Theophylline–acid stoichiometry in anhydrous form. [b]Theophylline–acid–water stoichiometry in hydrate form. [c]The theophylline–citric acid cocrystal formation was confirmed by a PXRD experiment, but it was not possible to grow a crystal for an SXRD measurement and so the 1:1 stoichiometry is hypothetical.

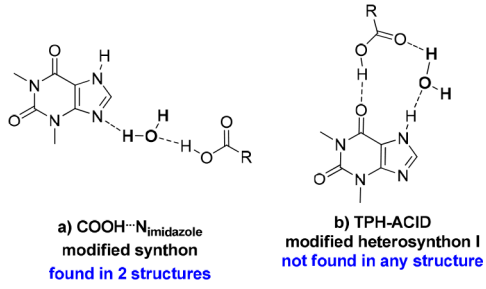

Figure 15. Specific alkaloid–acid synthons identified in TPH systems, in which the water molecule is involved.

are not present in the crystal lattice of the above substances (Figures 13.1c and 13.3a). In the TPH·HMLA cocrystal, by a COOH···$N_{imidazole}$ interaction with the external carboxylic group from acid molecule participation, TPH–acid heterosynthons I and II are formed (Figure 13.2.g, 13.2.c, and 13.2.d, respectively). In turn, the hydrogen bond network in $(TPH)^+ \cdot (HMLA)^- \cdot 2H_2O$ is quite complex and it would be very difficult to predict the supramolecular synthons present in this structure, unlike the case for the anhydrous equivalent. In the dihydrate phase the $COO^-\cdots H-N_{imidazole}$ hydrogen bond is formed (COOH···$N_{imidazole}$ synthon with proton transfer), this time with the internal carboxyl group of HMLA participation. The TPH–acid heterosynthon I (Figure 13.2c), observed in three structures containing theophylline, in $(TPH)^+ \cdot (HMLA)^- \cdot 2H_2O$ is slightly modified by interjecting one solvent molecule (Figure 15b, the $R_3^3(11)$ motif). Additionally, the carboxyl–carboxylate dimer with the water molecule as a bridge between both groups was identified (Figure 16b).

Theophylline and hemimellitic acid can form both neutral (cocrystal 1:1) and ionized complexes (salt dihydrate 1:1:2); thus, we observe two different ionization states for the same acid–base pair. This situation is possible when the ΔpK_a value for two substances (in this case $\Delta pK_a = 0.7$, Table 4) is in the

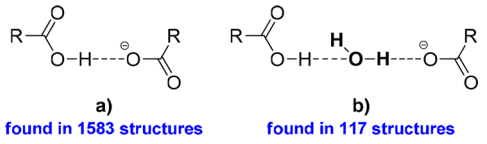

Figure 16. Carboxyl–carboxylate dimer (a) and its equivalent with a built-in water molecule (b).

range −1 to 4, where it is often difficult to predict whether a cocrystal or salt will be formed.[82] Several examples of acid–base that can form both neutral and ionized complexes were found and are shown in Table 7. Interestingly, no coformer was found in the literature or in the CSD database that in combination with a purine derivative would create both forms.

Table 7. Examples of Acid–Base Pairs That under Various Conditions Can Form a Neutral or Ionized Complex

base–acid pair	stoichiometry of neutral base–acid complex	stoichiometry of ionic base–acid complex
pyridine–formic acid[83]	1:1	1:4
pyridine–3,5-dinitrobenzoic acid[84]	1:2	1:1:1 with water
2,3-lutidine–fumaric acid[85]	2:1	1:2
sulfamethazine–saccharin[86]	1:1[87]	1:1[87,88]

3.3.3. Caffeine Derivatives. Caffeine forms a cocrystal with trimesic acid and a cocrystal hydrate with hemimellitic acid. In both complexes, as expected, one of the carboxyl groups is hydrogen-bonded via an COOH···$N_{imidazole}$ interaction with the imidazole nitrogen atom of the alkaloid molecule (Figure 13.2g), while in the caffeine complex with hemimellitic acid the internal carboxyl group of the acid takes part in this hydrogen bond formation. The carbonyl oxygen atoms near the pyrimidine ring in the caffeine molecule do not take part in the alkaloid–acid synthon formation by strong hydrogen bonds (Figure 13.2e and 13.2f), because two remaining carboxyl groups that could be hydrogen-bond donors to these atoms are engaged in acid–acid synthon formation. In the caffeine trimesic acid cocrystal, classical cyclic carboxylic acid dimers $R_2^2(8)$ are formed (Figure 13.3a). In caffeine hemimellitic acid monohydrate, one of the O–H(carboxyl)···O=C(carboxyl) interactions incorporates up to one water molecule and an $R_3^3(10)$ motif was observed (Figure 17).

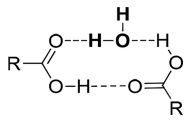

Figure 17. Cyclic dimer composed of two carboxylic acid groups and a water molecule, a so-called moderately successful synthon.[89] This motif was found in 38 structures in the CSD database.

These synthons are not the same, but equivalent and $R_2^2(8)$ and $R_3^3(10)$ ring formation can be regarded as synthon success in CAF·TMSA and moderate synthon success in CAF·HMLA·H_2O, respectively.[69,89]

3.4. Relationship between Donor–Acceptor Ratio and Hydrate Formation. At the cocrystal design stage, on the basis of the structure of the substrates used, the ratio of available donors to hydrogen bond acceptors can be

https://dx.doi.org/10.1021/acs.cgd.0c01242
Cryst. Growth Des. 2021, 21, 396–413

determined (d/a ratio). One of the Etter rules says that all good donors and all good hydrogen bond acceptors should participate in hydrogen bonding.[90] For TBR or TPH systems with a selected tricarboxylic acid, the d/a ratio is 4:9, while that for CAF is 3:9.

One of the first studies on the dependence of hydrate formation on the number of groups capable of forming hydrogen bonds was undertaken by Desiraju, who showed that more than half of the hydrated substances have a d/a ratio of less than 0.5.[91] However, van de Streek and Motherwell later showed that the average d/a ratios in hydrated and anhydrous structures (so far deposited in the CSD database) were 0.63 and 0.28, respectively, which would contradict Desiraju's hypothesis that low d/a ratio is the cause of water incorporation into the crystal lattice.[92] On the other hand, they showed that in hydrated structures the average number of unsatisfied acceptors is significantly reduced in comparison to the anhydrous systems, suggesting that water compensates for the lack or small amount of hydrogen bond donors by reducing the number of unsatisfied acceptors. Bi- or trifurcated and/or weak C−H···A hydrogen bonds (A = O, N) should form when the number of acceptors significantly exceeds the number of donors, and no solvent molecules are present in the crystal lattice.[91]

3.4.1. Theobromine Systems. In the case of TBR, both anhydrous systems were obtained. This was surprising for the TBR·HMLA cocrystal, because the donor groups in hemimellitic acid are closely located and the solvent could prevent steric hindrance. However, the formation of 1D ribbons by these molecules in TBR·HMLA, connected to the neighboring by many weak interactions (Table S7), prevented the incorporation of water molecules into the crystal network. Despite the fact that in both complexes the two carbonyl oxygen atoms in the acid molecule and, additionally, the *endo*-oxygen atoms of the alkaloid in TBR·HMLA are good acceptors and do not participate in the strong contact formation, they form weak C−H···O interactions, and it was not necessary to incorporate water molecules into the crystal lattice of both complexes (Figures 5b and 9c).

3.4.2. Theophylline Systems. Theophylline has both cocrystal and dihydrate forms with both acids, where the d/a ratios are 4:9 and 8:11, respectively. It can be concluded that the formation of hydrated forms of TPH with the above acids will result in better use of all acceptors for the formation of strong hydrogen bonds than in the anhydrous forms. This statement is true when TMSA was used. Two acceptors remain unsatisfied in TPH·TMSA, i.e., the *endo*-oxygen atom in TPH and one carbonyl atom in the TMSA molecule (Figure 6b), while in the dihydrate only one carbonyl oxygen atom in TPH does not form a strong contact (Figure 7b). It should also be noted that the embedded water molecules create channels, which definitely increased the role of strong interactions in stabilizing the three-dimensional structure of TPH·TMSA·$2H_2O$ (Figure 7c,d).

In the TPH·HMLA cocrystal, two carbonyl oxygen atoms in HMLA molecules do not form strong hydrogen bonds (Figure 10b). The formation of an ionic form with embedded water molecules, $(TPH)^+\cdot(HMLA)^-\cdot 2H_2O$, leads to a complex network of hydrogen bond formation, where also two oxygen atoms are unsatisfied acceptors, but this time the *endo*-oxygen atom in the TPH molecule and one carbonyl oxygen atom in the HMLA molecule do not form strong contacts (Figure 11b,c). Thus, after the hydrate formation, the same number of unsatisfied acceptors remained as in the anhydrous form, despite the number of donors being balanced against the number of acceptors. Additionally, the cocrystallizations carried out from the solution show that it is easier to obtain an anhydrous form than a hydrated form, while TPH·HMLA could only be obtained by grinding (Figure 4.3). $(TPH)^+\cdot(HMLA)^-\cdot 2H_2O$ was formed in several cocrystallizations from methanol−water solution, but the strict conditions for its preparation could not be determined. In addition, after some time, the crystals of this compound became pulverized. In this case, the incorporation of water molecules improved the donor−acceptor balance and caused strong hydrogen bonds to form a two-dimensional network in the dihydrate form (as opposed to that in TPH·HMLA—in one direction) but also worsened the stability of the hydrated form in comparison to the anhydrous form.

3.4.3. Caffeine Systems. Caffeine forms a cocrystal with TMSA and a monohydrate with HMLA, which was not surprising. Here, the isomerism of acids plays an important role. In both examples, the COOH···$N_{imidazole}$ heterosynthon was formed. An infinite one-dimensional structural motif of hydrogen bonds between carboxyl groups is also observed in both systems (Figures 8c and 12b). The difference is that in the CAF·TMSA cocrystal typical homosynthons were formed (Figure 13.3a) and, apart from the COOH···$N_{imidazole}$ hydrogen bond, the remaining synthons are weak interactions. The incorporation of solvent molecules into the carboxylic synthon of CAF·HMLA·H_2O (Figure 17) not only balances the donor−acceptor ratio to 0.5 but also prevents the formation of unfavorable interactions between adjacent CAF molecules noncovalently connected to subsequent HMLA molecules and is a link between three acid molecules, where one acid molecule is located in the neighboring ribbon (Figure 12b). In both cases, the carbonyl oxygen atoms near the pyrimidine ring of CAF, being good acceptors, form weak interactions. It should be mentioned that even neat grinding of CAF with HMLA leads to cocrystal hydrate formation (Figure 4.2).

3.5. Solubility Studies. The solubilities of all materials has been evaluated by using UV−vis spectroscopy. The results summarized in Table 8 clearly show that the obtained complexes with hemimellitic acid as a coformer (30.6 g L^{-1}) have higher solubility in comparison to those with trimesic acid (26.3 g L^{-1}). Both of the theobromine cocrystals, TBR·HMLA and TBR·TMSA, show an improved solubility in comparison

Table 8. Solubility of Theobromine, Theophylline, and Caffeine Cocrystals in Water[a]

alkaloid−acid system	absorption solubility (g L^{-1})
Theobromine Cocrystals	
TBR·TMSA	0.35 (×1.06)
TBR·HMLA	2.36 (×7.15)
Theophylline Cocrystals	
TPH·TMSA	2.07 (×0.25)
TPH·TMSA·$2H_2O$	2.01 (×0.24)
TPH·HMLA	9.6 (×1.16)
$(TPH)^+\cdot(HMLA)^-\cdot 2H_2O$	147.9 (×17.82)
Caffeine Cocrystals	
CAF·TMSA	1.37 (×0.09)
CAF·HMLA·H_2O	4.86 (×0.30)

[a]The increase relative to TBR, TPH, and CAF is shown in parentheses, respectively.

https://dx.doi.org/10.1021/acs.cgd.0c01242
Cryst. Growth Des. 2021, 21, 396−413

to the pure TBR. TBR·HMLA shows about a 7-fold increase in the solubility of TBR, whereas for TBR·TMSA this improvement is very slight and similar to the solubility of TBR. Solubilities of TPH cocrystals with trimesic acid as a coformer, TPH·TMSA and TPH·TMSA·2H_2O, are comparable and show about a 4-fold decrease in comparison to the pure TPH. Unlike TPH cocrystals with TMSA, samples with HMLA as a coformer show an increase in solubility. The solubility of TPH·HMLA is slightly higher, 1.16 times. As expected, $(TPH)^+\cdot(HMLA)^-\cdot 2H_2O$ is the most highly soluble compound among theophylline systems and shows 17.8 times the solubility of TPH. The results obtained for CAF cocrystals show a decreased solubility in both samples in comparison to pure CAF. CAF·TMSA and CAF·HMLA·H_2O show about 12- and 3.3-fold decreases in the solubility of CAF, respectively.

4. CONCLUSIONS

Trimesic acid (TMSA) and hemimellitic acid (HMLA), which are structural isomers, were used as coformers in purine alkaloid cocrystallization. Eight solids were obtained and structurally characterized. Theobromine forms cocrystals in a 1:1 stoichiometric ratio with both acids (TBR·TMSA and TBR·HMLA). Caffeine forms the cocrystal CAF·TMSA and cocrystal hydrate CAF·HMLA·H_2O with trimesic and hemimellitic acid, respectively. Theophylline with each acid forms both anhydrous (TPH·TMSA and TPH·HMLA) and dihydrate forms (TPH·TMSA·2H_2O and $(TPH)^+\cdot(HMLA)^-\cdot 2H_2O$), in which we do not observe proton transfer, except for $(TPH)^+\cdot(HMLA)^-\cdot 2H_2O$. Theophylline with hemimellitic acid is an interesting acid−base pair that forms a molecular or proton transfer complex depending on the crystallization conditions. No similar case was found in the literature or in the CSD database with a purine alkaloid as base. All of the above substances were synthesized by cocrystallization from solution. Mechanochemical methods were also applied to prepare the described complexes and seven of the eight substances, except for $(TPH)^+\cdot(HMLA)^-\cdot 2H_2O$, were successfully obtained by grinding. Solubility studies were performed using UV−vis spectroscopy. The complex formation with hemimellitic acid improves the purine alkaloid solubility in water in comparison to trimesic acid. Both cocrystals with theobromine are more soluble in water than the pure alkaloid. Theophylline complexes with trimesic acid are less soluble in water, but complexes with hemimellitic acid are more soluble in water than pure alkaloid. The most water soluble compound of all presented in this work is the salt dihydrate $(TPH)^+\cdot(HMLA)^-\cdot 2H_2O$. Both caffeine complexes are characterized by less solubility in water than pure xanthine. The incorporation of water molecules into the crystal lattice is not only to balance the donor−acceptor ratio in the obtained complexes but also to better use good acceptors for the formation of strong hydrogen bonds (TPH·TMSA·2H_2O) or to prevent the formation of steric hindrance (CAF·HMLA·H_2O). In the case of the the complex $(TPH)^+\cdot(HMLA)^-\cdot 2H_2O$, despite the improvement in the donor−acceptor balance after hydrate formation, first, this complex was very difficult to obtain, and second, it was less stable in comparison to the nonhydrated form TPH·HMLA.

The crystal structures of the eight substances with purine alkaloids were determined using single-crystal X-ray diffraction methods, and all the supramolecular motifs with alkaloid and acid molecule participation were identified and analyzed. The alkaloid−acid and acid−acid synthons were the most expected synthons to be found in the described structures. The alkaloid−alkaloid homosynthons are present only in the TBR·TMSA cocrystal, which is consistent with the above assumption. Hydrogen bonds of COOH···$N_{imidazole}$ type were found in each complex, which was obvious, but in TPH·TMSA·2H_2O, the water molecule links between the carboxyl group and imidazole moiety in this interaction. It should be noted that, rather, this intermolecular contact is formed by the internal carboxyl group of hemimellitic acid, which can be observed in three out of the four systems with this acid described in this work. The remaining synthons have been characterized and analyzed in terms of their frequency in the structures of purine alkaloids deposited in the CSD base so far. The structural analysis shows that in some cases noncovalent interactions and the arrangement of the molecules in the crystal lattice can be easily predicted, while the diversity of supramolecular synthons indicates that structure design is often difficult. This shows how important it is to study self-organization processes in systems with many functional groups.

■ ASSOCIATED CONTENT

Supporting Information

The Supporting Information is available free of charge at https://pubs.acs.org/doi/10.1021/acs.cgd.0c01242.

Solution-based and grinding cocrystallization conditions, additional details of crystal structure solution and refinement, UV−vis measurements with steady-state absorption curves, crystallographic data, hydrogen bonds and stacking geometry in the described cocrystals, and Hirshfeld surface analysis and fingerprint plots (PDF)

Accession Codes

CCDC 2019776−2019783 contain the supplementary crystallographic data for this paper. These data can be obtained free of charge via www.ccdc.cam.ac.uk/data_request/cif, or by emailing data_request@ccdc.cam.ac.uk, or by contacting The Cambridge Crystallographic Data Centre, 12 Union Road, Cambridge CB2 1EZ, UK; fax: +44 1223 336033.

■ AUTHOR INFORMATION

Corresponding Author

M. R. Gołdyn − *Faculty of Chemistry, Adam Mickiewicz University, 61-614 Poznań, Poland;* orcid.org/0000-0003-2282-9816; Email: mateusz.goldyn@amu.edu.pl

Authors

D. Larowska − *Faculty of Chemistry, Adam Mickiewicz University, 61-614 Poznań, Poland*

E. Bartoszak-Adamska − *Faculty of Chemistry, Adam Mickiewicz University, 61-614 Poznań, Poland*

Complete contact information is available at: https://pubs.acs.org/10.1021/acs.cgd.0c01242

Notes

The authors declare no competing financial interest.

■ ACKNOWLEDGMENTS

The authors want to acknowledge financial support from the European Union through grant no. POWR.03.02.00-00-I026/16 cofinanced by the European Union through the European Social Fund under the Operational Program Knowledge Education Development. We thank Professor Maria Gdaniec

for fruitful discussions on twinned crystals. Our thanks go also to Dr. Agnieszka Kiliszek and Martyna Pluta from the Institute of Bioorganic Chemistry of the Polish Academy of Sciences in Poznań for providing the XtaLAB Synergy-R diffractometer for $(TPH)^{+}\cdot(HMLA)^{-}\cdot 2H_2O$ crystal data collection.

REFERENCES

(1) Aitipamula, S.; Banerjee, R.; Bansal, A. K.; Biradha, K.; Cheney, M. L.; Choudhury, A. R.; Desiraju, G. R.; Dikundwar, A. G.; Dubey, R.; Duggirala, N.; Ghogale, P. P.; Ghosh, S.; Goswami, P. K.; Goud, N. R.; Jetti, R. R. K. R.; Karpinski, P.; Kaushik, P.; Kumar, D.; Kumar, V.; Moulton, B.; Mukherjee, A.; Mukherjee, G.; Myerson, A. S.; Puri, V.; Ramanan, A.; Rajamannar, T.; Reddy, C. M.; Rodriguez-Hornedo, N.; Rogers, R. D.; Row, T. N. G.; Sanphui, P.; Shan, N.; Shete, G.; Singh, A.; Sun, C. C.; Swift, J. A.; Thaimattam, R.; Thakur, T. S.; Kumar Thaper, R.; Thomas, S. P.; Tothadi, S.; Vangala, V. R.; Variankaval, N.; Vishweshwar, P.; Weyna, D. R.; Zaworotko, M. J. Polymorphs, Salts, and Cocrystals: What's in a Name? *Cryst. Growth Des.* **2012**, *12*, 2147−2152.

(2) Kumar, S.; Nanda, A. Pharmaceutical Cocrystals: An Overview. *Indian J. Pharm. Sci.* **2017**, *79*, 858−871.

(3) FDA/CDER/Stewart, F. Regulatory Classification of Pharmaceutical Co-Crystals Guidance for Industry. 7.

(4) Mandal, S.; Mukhopadhyay, T. K.; Mandal, N.; Datta, A. Hierarchical Noncovalent Interactions between Molecules Stabilize Multicomponent Cocrystals. *Cryst. Growth Des.* **2019**, *19*, 4802−4809.

(5) Bauzá, A.; Mooibroek, T. J.; Frontera, A. Towards Design Strategies for Anion−π Interactions in Crystal Engineering. *CrystEngComm* **2016**, *18*, 10−23.

(6) Vishweshwar, P.; McMahon, J. A.; Bis, J. A.; Zaworotko, M. J. Pharmaceutical Co-Crystals. *J. Pharm. Sci.* **2006**, *95*, 499−516.

(7) Shaikh, R.; Singh, R.; Walker, G. M.; Croker, D. M. Pharmaceutical Cocrystal Drug Products: An Outlook on Product Development. *Trends Pharmacol. Sci.* **2018**, *39*, 1033−1048.

(8) Duggirala, N. K.; Perry, M. L.; Almarsson, Ö.; Zaworotko, M. J. Pharmaceutical Cocrystals: Along the Path to Improved Medicines. *Chem. Commun.* **2016**, *52*, 640−655.

(9) Desiraju, G. R. Crystal Engineering: A Holistic View. *Angew. Chem., Int. Ed.* **2007**, *46*, 8342−8356.

(10) Corpinot, M. K.; Bučar, D.-K. A Practical Guide to the Design of Molecular Crystals. *Cryst. Growth Des.* **2019**, *19*, 1426−1453.

(11) Kavanagh, O. N.; Croker, D. M.; Walker, G. M.; Zaworotko, M. J. Pharmaceutical Cocrystals: From Serendipity to Design to Application. *Drug Discovery Today* **2019**, *24*, 796−804.

(12) Amidon, G. L.; Lennernäs, H.; Shah, V. P.; Crison, J. R. A Theoretical Basis for a Biopharmaceutic Drug Classification: The Correlation of in Vitro Drug Product Dissolution and in Vivo Bioavailability. *Pharm. Res.* **1995**, *12*, 413−420.

(13) Song, Y.; Wang, L.-Y.; Liu, F.; Li, Y.-T.; Wu, Z.-Y.; Yan, C.-W. Simultaneously Enhancing the *in Vitro*/*in Vivo* Performances of Acetazolamide Using Proline as a Zwitterionic Coformer for Cocrystallization. *CrystEngComm* **2019**, *21*, 3064−3073.

(14) Patel, D. J.; Puranik, P. K. Pharmaceutical Co-Crystal: An Emerging Technique to Enhance Physicochemical Properties of Drugs. *Int. J. ChemTech Res.* **2020**, *13*, 283−290.

(15) Najar, A. A.; Azim, Y. Pharmaceutical Co-Crystals: A New Paradigm of Crystal Engineering. *J. Indian Inst. Sci.* **2014**, *94*, 25.

(16) Lohani, S.; Cooper, H.; Jin, X.; Nissley, B. P.; Manser, K.; Rakes, L. H.; Cummings, J. J.; Fauty, S. E.; Bak, A. Physicochemical Properties, Form, and Formulation Selection Strategy for a Biopharmaceutical Classification System Class II Preclinical Drug Candidate. *J. Pharm. Sci.* **2014**, *103*, 3007−3021.

(17) Shah, V. P.; Amidon, G. L. G.L.; Amidon, H.; Lennernas, V. P.; Shah; Crison, J. R. A Theoretical Basis for a Biopharmaceutic Drug Classification: The Correlation of In Vitro Drug Product Dissolution and In Vivo Bioavailability, Pharm Res 12, 413−420, 1995—Backstory of BCS. *AAPS J.* **2014**, *16*, 894−898.

(18) Aitipamula, S.; Vangala, V. R. X-Ray Crystallography and Its Role in Understanding the Physicochemical Properties of Pharmaceutical Cocrystals. *J. Indian Inst. Sci.* **2017**, *97*, 227−243.

(19) Khadka, P.; Ro, J.; Kim, H.; Kim, I.; Kim, J. T.; Kim, H.; Cho, J. M.; Yun, G.; Lee, J. Pharmaceutical Particle Technologies: An Approach to Improve Drug Solubility, Dissolution and Bioavailability. *Asian J. Pharm. Sci. (Amsterdam, Neth.)* **2014**, *9*, 304−316.

(20) da Fonseca Antunes, A. B.; De Geest, B. G.; Vervaet, C.; Remon, J. P. Solvent-Free Drug Crystal Engineering for Drug Nano- and Micro Suspensions. *Eur. J. Pharm. Sci.* **2013**, *48*, 121−129.

(21) Rizvi, S. A. A.; Saleh, A. M. Applications of Nanoparticle Systems in Drug Delivery Technology. *Saudi Pharm. J.* **2018**, *26*, 64−70.

(22) Grzesiak, A. L.; Lang, M.; Kim, K.; Matzger, A. J. Comparison of the Four Anhydrous Polymorphs of Carbamazepine and the Crystal Structure of Form I**Supplementary Material: X-ray Crystallographic Information File (CIF) of Triclinic CBZ (Form I) Is Available. *J. Pharm. Sci.* **2003**, *92*, 2260−2271.

(23) Chaudhari, S.; Nikam, S. A.; Khatri, N.; Wakde, S. CO-CRYSTALS: A REVIEW. *J. Drug Delivery Ther.* **2018**, *8*, 350−358.

(24) Roy, P.; Ghosh, A. Mechanochemical Cocrystallization to Improve the Physicochemical Properties of Chlorzoxazone. *CrystEngComm* **2020**, *22*, 4611−4620.

(25) Viertelhaus, M.; CHIODO, T.; Salvador, B.; Vossen, M.; Hafner, A.; Hintermann, T.; Weishaar, W.; Hellmann, R. Multi-Component Crystals of Vismodegib and Selected Co-Crystal Formers or Solvents. WO2016020324A1, February 11, 2016.

(26) Connelly, P. R.; Collier, S.; Tauber, M. Co-Crystals and Pharmaceutical Compositions Comprising the Same. US8372846B2, February 12, 2013.

(27) Pi, J.; Wang, S.; Li, W.; Kebebe, D.; Zhang, Y.; Zhang, B.; Qi, D.; Guo, P.; Li, N.; Liu, Z. A Nano-Cocrystal Strategy to Improve the Dissolution Rate and Oral Bioavailability of Baicalein. *Asian J. Pharm. Sci. (Amsterdam, Neth.)* **2019**, *14*, 154−164.

(28) Bezerra, B. P.; Pogoda, D.; Perry, M. L.; Vidal, L. M. T.; Zaworotko, M. J.; Ayala, A. P. Cocrystal Polymorphs and Solvates of the Anti- *Trypanosoma Cruzi* Drug Benznidazole with Improved Dissolution Performance. *Cryst. Growth Des.* **2020**, *20*, 4707−4718.

(29) Rai, S. K.; Gunnam, A.; Mannava, M. K. C.; Nangia, A. K. Improving the Dissolution Rate of the Anticancer Drug Dabrafenib. *Cryst. Growth Des.* **2020**, *20*, 1035−1046.

(30) Arabiani, M. R.; K, B. R.; Bhunia, S.; Teja, P. K.; Lodagekar, A.; Chavan, R. B.; Shastri, N. R.; Reddy, C. M.; Shelat, P.; Dave, D. Brexpiprazole−Catechol Cocrystal: Structure Elucidation, Excipient Compatibility and Stability. *CrystEngComm* **2019**, *21*, 6703−6708.

(31) Jirát, J.; Ondo, D.; Babor, M.; Ridvan, L.; Šoóš, M. Complex Methodology for Rational Design of Apremilast-Benzoic Acid Co-Crystallization Process. *Int. J. Pharm. (Amsterdam, Neth.)* **2019**, *570*, 118639.

(32) Co-Crystals of Ribociclib and Co-Crystals of Ribociclib Mono-Succinate, Preparation Method Therefor, Compositions Thereof, and Uses Thereof. WO2019062854A1, April 4, 2019.

(33) Souza, F. E. S.; Khalili, B.; Rantanen, K. A. Crystalline Form of Lumacaftor. 20190112299, April 18, 2019.

(34) Oracz, M.; SKOCZEN, P. Cocrystals of Apremilast. EP3339292A1, June 27, 2018.

(35) Zhou, Z.; Li, W.; Sun, W.-J.; Lu, T.; Tong, H. H. Y.; Sun, C. C.; Zheng, Y. Resveratrol Cocrystals with Enhanced Solubility and Tabletability. *Int. J. Pharm. (Amsterdam, Neth.)* **2016**, *509*, 391−399.

(36) Venkata Narasayya, S.; Maruthapillai, A.; Sundaramurthy, D.; Arockia Selvi, J.; Mahapatra, S. Preparation, Pharmaceutical Properties and Stability of Lesinurad Co-Crystals and Solvate. *Mater. Today: Proc.* **2019**, *14*, 532−544.

(37) Tartaric Acid Cariliprazine and Preparation Method Thereof and Medical Usage. CN105218484B, February 23, 2018.

(38) Co-Crystal of Olaparib and Urea and Preparation Method Therefor. WO2016165650A1, October 20, 2016.

(39) Albrecht, W.; Geier, J.; Rabe, S.; Palacios, D. P. Co-Crystals of Ibrutinib with Carboxylic Acids. US10377758B2, August 13, 2019.

https://dx.doi.org/10.1021/acs.cgd.0c01242
Cryst. Growth Des. 2021, 21, 396−413

(40) CZYZEWSKI, A. M. c/o P. G. R. & D.; Gao, D. P. G. R. Non-Hygroscopic Formulation Comprising a Hydroscopic Drug. EP1575563B1, February 14, 2007.
(41) Wang, Z.-Z.; Chen, J.-M.; Lu, T.-B. Enhancing the Hygroscopic Stability of *S*-Oxiracetam via Pharmaceutical Cocrystals. *Cryst. Growth Des.* **2012**, *12*, 4562−4566.
(42) Emami, S.; Siahi-Shadbad, M.; Adibkia, K.; Barzegar-Jalali, M. Recent Advances in Improving Oral Drug Bioavailability by Cocrystals. *BioImpacts* **2018**, *8*, 305−320.
(43) Raheem Thayyil, A.; Juturu, T.; Nayak, S.; Kamath, S. Pharmaceutical Co-Crystallization: Regulatory Aspects, Design, Characterization, and Applications. *Adv. Pharm. Bull.* **2020**, *10*, 203−212.
(44) Bolton, S.; Null, G. Caffeine Psychological Effects, Use and Abuse. *Orthomol. Psychiatry* **1981**, *10*, 202−211.
(45) Nehlig, A.; Daval, J.-L.; Debry, G. Caffeine and the Central Nervous System: Mechanisms of Action, Biochemical, Metabolic and Psychostimulant Effects. *Brain Res. Rev.* **1992**, *17*, 139−170.
(46) Nehlig, A. Is Caffeine a Cognitive Enhancer? *J. Alzheimer's Dis.* **2010**, *20*, S85−S94.
(47) Schultze-Werninghaus, G.; Meier-Sydow, J. The Clinical and Pharmacological History of Theophylline: First Report on the Bronchospasmolytic Action in Man by S. R. Hirsch in Frankfurt (Main) 1922. *Clin. Exp. Allergy* **1982**, *12*, 211−215.
(48) Sarma, B.; Saikia, B. Hydrogen Bond Synthon Competition in the Stabilization of Theophylline Cocrystals. *CrystEngComm* **2014**, *16*, 4753−4765.
(49) Sanphui, P.; Nangia, A. Salts and Co-Crystals of Theobromine and Their Phase Transformations in Water. *J. Chem. Sci.* **2014**, *126*, 1249−1264.
(50) All about Chocolate−Science; http://www.xocoatl.org/science.htm (accessed July 3, 2020).
(51) Groom, C. R.; Bruno, I. J.; Lightfoot, M. P.; Ward, S. C. The Cambridge Structural Database. *Acta Crystallogr., Sect. B: Struct. Sci., Cryst. Eng. Mater.* **2016**, *72*, 171−179.
(52) Shefter, E.; Higuchi, T. Dissolution Behavior of Crystalline Solvated and Nonsolvated Forms of Some Pharmaceuticals. *J. Pharm. Sci.* **1963**, *52*, 781−791.
(53) Sigma Aldrich, Caffeine (Anhydrous), Product Number C0750, Product Information, https://www.sigmaaldrich.com/content/dam/sigma-aldrich/docs/Sigma-Aldrich/Product_Information_Sheet/c0750pis.pdf (accessed Auguest 17, 2020).
(54) Desiraju, G. R. Supramolecular Synthons in Crystal Engineering—A New Organic Synthesis. *Angew. Chem., Int. Ed. Engl.* **1995**, *34*, 2311−2327.
(55) *CrysAlisPro Software System, Version 1.171.40.67a*; Rigaku Corporation: Wroclaw, Poland, 2019.
(56) Sheldrick, G. M. *SHELXT* − Integrated Space-Group and Crystal-Structure Determination. *Acta Crystallogr., Sect. A: Found. Adv.* **2015**, *71*, 3−8.
(57) Sheldrick, G. M. Crystal Structure Refinement with *SHELXL*. *Acta Crystallogr., Sect. C: Struct. Chem.* **2015**, *71*, 3−8.
(58) Dolomanov, O. V.; Bourhis, L. J.; Gildea, R. J.; Howard, J. A. K.; Puschmann, H. *OLEX2*: A Complete Structure Solution, Refinement and Analysis Program. *J. Appl. Crystallogr.* **2009**, *42*, 339−341.
(59) Farrugia, L. J. *WinGX* and *ORTEP for Windows*: An Update. *J. Appl. Crystallogr.* **2012**, *45*, 849−854.
(60) Macrae, C. F.; Sovago, I.; Cottrell, S. J.; Galek, P. T. A.; McCabe, P.; Pidcock, E.; Platings, M.; Shields, G. P.; Stevens, J. S.; Towler, M.; Wood, P. A. *Mercury 4.0*: From Visualization to Analysis, Design and Prediction. *J. Appl. Crystallogr.* **2020**, *53*, 226−235.
(61) Knížek, K. *Kdif Software*; Https://Www.Fzu.Cz/~knizek/Kalvados/Download.Html (accessed on July 11, 2020).
(62) Turner, M. J.; McKinnon, J. J.; Wolff, S. K.; Grimwood, D. J.; Spackman, P. R.; Jayatilaka, D.; Spackman, M. A. *CrystalExplorer17*; University of Western Australia: 2017.
(63) Hirshfeld, F. L. Bonded-Atom Fragments for Describing Molecular Charge Densities. *Theoret. Chim. Acta* **1977**, *44*, 129−138.
(64) Bruno, I. J.; Cole, J. C.; Edgington, P. R.; Kessler, M.; Macrae, C. F.; McCabe, P.; Pearson, J.; Taylor, R. New Software for Searching the Cambridge Structural Database and Visualizing Crystal Structures. *Acta Crystallogr., Sect. B: Struct. Sci.* **2002**, *58*, 389−397.
(65) Cruz-Cabeza, A. J. Acid−Base Crystalline Complexes and the PKa Rule. *CrystEngComm* **2012**, *14*, 6362.
(66) Pereira, J. F. B.; Magri, A.; Quental, M. V.; Gonzalez-Miquel, M.; Freire, M. G.; Coutinho, J. A. P. Alkaloids as Alternative Probes To Characterize the Relative Hydrophobicity of Aqueous Biphasic Systems. *ACS Sustainable Chem. Eng.* **2016**, *4*, 1512−1520.
(67) Perez-Martinez, I.; Sagrado, S.; Medina-Hernandez, M.J. A Rapid Procedure for the Determination of Caffeine, Theophylline and Theobromine in Urine by Micellar Liquid Chromatography and Direct Sample Injection. *Anal. Chim. Acta* **1995**, *304*, 195−201.
(68) Ripin, D. H.; Evans, D. A. PKa's of Inorganic and Oxo-Acids Chem 206, https://pdfslide.net/documents/dh-ripin-da-evans-pkas-of-inorganic-and-oxo-acids-chem-206.html (accessed on December 28, 2020).
(69) Sander, J. R. G.; Bučar, D.-K.; Henry, R. F.; Giangiorgi, B. N.; Zhang, G. G. Z.; MacGillivray, L. R. Masked Synthons' in Crystal Engineering: Insulated Components in Acetaminophen Cocrystal Hydrates. *CrystEngComm* **2013**, *15*, 4816.
(70) Abosede, O. O.; Gordon, A. T.; Dembaremba, T. O.; Lorentino, C. M. A.; Frota, H. F.; Santos, A. L. S.; Hosten, E. C.; Ogunlaja, A. S. Trimesic Acid−Theophylline and Isopthalic Acid−Caffeine Cocrystals: Synthesis, Characterization, Solubility, Molecular Docking, and Antimicrobial Activity. *Cryst. Growth Des.* **2020**, *20*, 3510−3522.
(71) D'Ascenzo, L.; Auffinger, P. A Comprehensive Classification and Nomenclature of Carboxyl−Carboxyl(Ate) Supramolecular Motifs and Related Catemers: Implications for Biomolecular Systems. *Acta Crystallogr., Sect. B: Struct. Sci., Cryst. Eng. Mater.* **2015**, *71*, 164−175.
(72) Ford, K. A.; Ebisuzaki, Y.; Boyle, P. D. Methylxanthines. II. Anhydrous Theobromine. *Acta Crystallogr., Sect. C: Cryst. Struct. Commun.* **1998**, *54*, 1980−1983.
(73) Gołdyn, M.; Larowska, D.; Nowak, W.; Bartoszak-Adamska, E. Theobromine Cocrystals with Monohydroxybenzoic Acids − Synthesis, X-Ray Structural Analysis, Solubility and Thermal Properties. *CrystEngComm* **2019**, *21*, 5721−5732.
(74) Gołdyn, M.; Larowska, D.; Nowak, W.; Bartoszak-Adamska, E. Synthon Hierarchy in Theobromine Cocrystals with Hydroxybenzoic Acids as Coformers. *CrystEngComm* **2019**, *21*, 7373−7388.
(75) Benghiat, V.; Leiserowitz, L. Molecular Packing Modes. Part VI. Crystal and Molecular Structures of Two Modifications of Tetrolic Acid. *J. Chem. Soc., Perkin Trans. 2* **1972**, *12*, 1763.
(76) Sanphui, P.; Bolla, G.; Das, U.; Mukherjee, A. K.; Nangia, A. Acemetacin Polymorphs: A Rare Case of Carboxylic Acid Catemer and Dimer Synthons. *CrystEngComm* **2013**, *15*, 34−38.
(77) Tobin, J. M.; Masuda, J. D. 2,6-Bis(Trifluoromethyl)Benzoic Acid. *Acta Crystallogr., Sect. E: Struct. Rep. Online* **2009**, *65*, o1217−o1217.
(78) Saikia, B.; Bora, P.; Khatioda, R.; Sarma, B. Hydrogen Bond Synthons in the Interplay of Solubility and Membrane Permeability/Diffusion in Variable Stoichiometry Drug Cocrystals. *Cryst. Growth Des.* **2015**, *15*, 5593−5603.
(79) Bučar, D.-K.; Henry, R. F.; Zhang, G. G. Z.; MacGillivray, L. R. Synthon Hierarchies in Crystal Forms Composed of Theophylline and Hydroxybenzoic Acids: Cocrystal Screening via Solution-Mediated Phase Transformation. *Cryst. Growth Des.* **2014**, *14*, 5318−5328.
(80) Wang, Z.-L.; Wei, L.-H. Theophylline−2,4-Dihydroxybenzoic Acid−Water (1/1/1). *Acta Crystallogr., Sect. E: Struct. Rep. Online* **2007**, *63*, o1681−o1682.
(81) Karki, S.; Friščić, T.; Jones, W.; Motherwell, W. D. S. Screening for Pharmaceutical Cocrystal Hydrates via Neat and Liquid-Assisted Grinding. *Mol. Pharmaceutics* **2007**, *4*, 347−354.

https://dx.doi.org/10.1021/acs.cgd.0c01242
Cryst. Growth Des. 2021, 21, 396−413

(82) Childs, S. L.; Stahly, G. P.; Park, A. The Salt−Cocrystal Continuum: The Influence of Crystal Structure on Ionization State. *Mol. Pharmaceutics* **2007**, *4*, 323−338.
(83) Wiechert, D.; Mootz, D. Crystal Structures of a 1/1 and a 1/4 Adduct of Pyridine and Formic Acid. *Angew. Chem., Int. Ed.* **1999**, *38*, 1974−1976.
(84) Arora, K. K.; PrakashaReddy, J.; Pedireddi, V. R. Pyridine Mediated Supramolecular Assemblies of 3,5-Dinitro Substituted Benzoic Acid, Benzamide and Benzonitrile. *Tetrahedron* **2005**, *61*, 10793−10800.
(85) Haynes, D. A.; Jones, W.; Motherwell, W. D. S. Cocrystallisation of Succinic and Fumaric Acids with Lutidines: A Systematic Study. *CrystEngComm* **2006**, *8*, 830.
(86) Cherukuvada, S.; Kaur, R.; Guru Row, T. N. Co-Crystallization and Small Molecule Crystal Form Diversity: From Pharmaceutical to Materials Applications. *CrystEngComm* **2016**, *18*, 8528−8555.
(87) Fu, X.; Li, J.; Wang, L.; Wu, B.; Xu, X.; Deng, Z.; Zhang, H. Pharmaceutical Crystalline Complexes of Sulfamethazine with Saccharin: Same Interaction Site but Different Ionization States. *RSC Adv.* **2016**, *6*, 26474−26478.
(88) Lu, E.; Rodríguez-Hornedo, N.; Suryanarayanan, R. A Rapid Thermal Method for Cocrystal Screening. *CrystEngComm* **2008**, *10*, 665.
(89) Bhatt, P. M.; Azim, Y.; Thakur, T. S.; Desiraju, G. R. Co-Crystals of the Anti-HIV Drugs Lamivudine and Zidovudine. *Cryst. Growth Des.* **2009**, *9*, 951−957.
(90) Etter, M. C. Encoding and Decoding Hydrogen-Bond Patterns of Organic Compounds. *Acc. Chem. Res.* **1990**, *23*, 120−126.
(91) Desiraju, G. R. Hydration in Organic Crystals: Prediction from Molecular Structure. *J. Chem. Soc., Chem. Commun.* **1991**, *6*, 426.
(92) van de Streek, J.; Motherwell, S. New Software for Searching the Cambridge Structural Database for Solvated and Unsolvated Crystal Structures Applied to Hydrates. *CrystEngComm* **2007**, *9*, 55−64.

https://dx.doi.org/10.1021/acs.cgd.0c01242
Cryst. Growth Des. 2021, 21, 396−413